REPORT DOCUMENTATION PAGE

Form Approved
OMB No. 0704-0188

Public reporting burden for this collection of information is estimated to average 1 hour per response, including the time for reviewing instructions, searching existing data sources, gathering and maintaining the data needed, and completing and reviewing the collection of information. Send comments regarding this burden estimate or any other aspect of this collection of information, including suggestions for reducing this burden, to Washington Headquarters Services, Directorate for Information Operations and Reports, 1215 Jefferson Davis Highway, Suite 1204, Arlington, VA 22202-4302, and to the Office of Management and Budget, Paperwork Reduction Project (0704-0188), Washington, DC 20503.

1. AGENCY USE ONLY (*Leave Blank*)	2. REPORT DATE	3. REPORT TYPE AND DATES COVERED
	1 October, 1997	Phase I Final Technical Report Feb. 15, 1997 to Aug. 15, 1997

4. TITLE AND SUBTITLE
Advanced Oxide Fibers and Coatings For High Temperature Composite Materials Applications

5. FUNDING NUMBERS
F49620-97-C-0003

6. AUTHORS
J.K.R. Weber, Waltraud M. Kriven*, Paul C. Nordine, Benjamin Cho, William Jellison, Dong Zhu*, Bradley R. Johnson*

7. PERFORMING ORGANIZATION NAME(S) AND ADDRESS(ES)
Containerless Research, Inc., 906 University Place, Evanston, IL 60201

* University of Illinois at Urbana-Champaign, Department of Materials Science and Engineering, 1304 West Green Street, Urbana, IL 61801

8. PERFORMING ORGANIZATION REPORT NUMBER
CRI 025AF-FR1

9. SPONSORING / MONITORING AGENCY NAME(S) AND ADDRESS(ES)
AFOSR/NA
Directorate of Aerospace and Material Sciences
110 Duncan Avenue, Suite B115
Bolling AFB, DC 20332-0001

10. SPONSORING / MONITORING AGENCY REPORT NUMBER

11. SUPPLEMENTARY NOTES

19980102 161

12a. DISTRIBUTION / AVAILABILITY STATEMENT
Unlimited

DISTRIBUTION STATEMENT A
Approved for public release
Distribution Unlimited

12b. DISTRIBUTION CODE

13. ABSTRACT *(Maximum 200 words)*

This research investigated the feasibility of a new process for manufacturing crystalline oxide fibers for high temperature structural applications. Glass fibers were pulled from undercooled melts and then crystallized under controlled heating conditions. The research emphasized mullite (Al6 Si2 O13) and yttrium-aluminum garnet - YAG (Y3 Al5 O12) compositions. Crystallization rates were several cm/s at 1200-2000 degrees C. Glass fibers of uniform diameter and no defects or visual imperfections exhibited tensile strength up to 5.3 GPa for the YAG-composition and 3.5 GPa for the mullite-composition. The strength of fibers crystallized below 1100 degrees C were 0.7 GPa for YAG and 1.3 GPa for mullite. Optimum crystallization conditions will be at higher temperatures where the crystallization rate is large compared to the rate of crystal nucleation, and rapid, economical synthesis of continuous single crystal fibers may be possible. Lower temperatures may be employed to obtain very fine-grained fibers. Phase II research would (i) synthesize long defect-free glass fibers, (ii) investigate kinetics of crystallization at higher temperatures where nucleation is suppressed, (iii) optimize mechanical properties achieved in the crystallization process, and (iv) provide high strength crystalline fiber materials for applications testing.

14. SUBJECT TERMS
Fibers, Oxides, Crystalline, Structural, Glass, Fiber Processing, Ceramic Matrix Composites

15. NUMBER OF PAGES
54

16. PRICE CODE

17. SECURITY CLASSIFICATION OF REPORT	18. SECURITY CLASSIFICATION OF THIS PAGE	19. SECURITY CLASSIFICATION OF ABSTRACT	20. LIMITATION OF ABSTRACT
Unclassified	Unclassified	Unclassified	

FINAL REPORT

October 1, 1997

ADVANCED OXIDE FIBERS AND COATINGS FOR HIGH TEMPERATURE COMPOSITE MATERIALS APPLICATIONS

Phase I Air Force STTR, Contract Number F49620-97-C-0003
Feb. 15, 1997 to Aug. 15, 1997

Principal Investigator: Dr. Richard Weber

Submitted by

Containerless Research, Inc.
Evanston, IL 60201-3149
Phone: 847/467-2678, Fax 847/467-2679
email: cri@containerless.com

Technical Monitor: Dr. Alexander Pechenik
AFOSR/NA, Directorate of Aerospace and Materials Sciences
110 Duncan Avenue, Suite B115, Bolling AFB, DC 20332-0001

Phone: 202/767-4962, Fax: 202/767-4988

Preface

This is the final technical report for research performed during the period February - August 1997 under an Air Force Phase I STTR Contract Number F49620-97-C-0003 with Containerless Research, Inc. (CRI) Dr. J.K.R. Weber of CRI was the Principal Investigator, assisted by Dr. Paul C. Nordine, Benjamin Cho, and William Jellison of CRI.

The University of Illinois at Champaign-Urbana (UIUC) was the research institution partner and subcontractor in this STTR project. Research at UIUC was directed by Professor Waltraud M. Kriven, assisted by Dr. Dong Zhu and Bradley R. Johnson.

Technical questions about this work should be directed to Dr. Weber or Dr. Nordine, and may also be directed to Professor Kriven at UIUC. Business and administrative questions should be directed to Dr. Nordine.

CONTAINERLESS RESEARCH, INC.

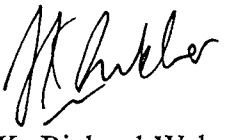

J.K. Richard Weber, Ph.D.
Director and Principal Scientist

Approved for

CONTAINERLESS RESEARCH, INC.

Paul C. Nordine
President

October 1, 1997

Table of Contents Page

Tables

Figures

1. EXECUTIVE SUMMARY

This Phase I STTR research project investigated the feasibility of a new process for manufacturing crystalline oxide fibers for high temperature structural applications. Glass fibers are formed by pulling from undercooled melts of sufficient viscosity to permit fiber pulling. The glass fibers are then crystallized under controlled heating conditions that yield high strength materials. Fibers from a wide variety of materials are available by this route since melt undercooling extends fiber pulling operations to many new materials. The Phase I project involved both fiber synthesis and fiber crystallization studies to achieve high strength crystalline materials. The research emphasized work on mullite ($Al_6Si_2O_{13}$) and yttrium-aluminum garnet or YAG ($Y_3Al_5O_{12}$) compositions. The methods are intrinsically fast, leading to inexpensive fiber manufacture.

The fibers were crystallized over a very wide range of conditions. Crystal growth rates were several cm/s at 1200-2000°C achieved when crystals nucleate from undercooled bulk melts. At lower temperatures obtained by slow heating, crystallization occurs at temperatures of 900-1000°C at rates of a few μm/s. Experiments were performed to investigate rapid crystallization of fibers at 1200-1400°C, where 30 mm long fibers were completely crystallized in less than five seconds. Analysis of these fibers to determine grain size, morphology, and surface characteristics is continuing and will be reported in the Phase II proposal.

Control of the fiber pulling process was developed to achieve high quality precursors for the crystallization experiments. The fibers were of uniform diameter. They exhibited no defects or visual imperfections in sections up to 20 cm long. The YAG-composition glass fiber strength was 5.3 GPa. Reproducible tensile fracture strengths equal to 3.5 GPa were obtained for mullite-composition glass fibers.

YAG fibers crystallized in slow heating experiments exhibited tensile strengths up to 0.7 GPa. Crystallized mullite fibers had tensile strengths up to 1.3 GPa. Optimum crystallization conditions are at higher temperatures where the crystallization rate is large compared to the rate of crystal nucleation. Directional crystallization, perhaps under tension, and on much longer fiber sections will be required to optimize the high-rate crystallization process.

Based on the Phase I results, the Phase II research plan is to (i) make continuous and defect-free glass fibers in pilot-scale quantities, (ii) investigate kinetics of crystallization at higher temperatures where crystal nucleation is suppressed, (iii) optimize the mechanical properties achieved in the crystallization process, and (iv) provide high strength crystalline fiber materials for applications testing. The possibility that the Phase II research will yield continuous single crystal fibers is discussed in the report.

2. INTRODUCTION

Oxide fiber-based ceramic composites (CMCs) are chemically stable at high temperatures in oxidizing environments. This makes them attractive candidates for applications in heat engines, thrust deflectors, rocket nozzles, and other high temperature structural components. Fibers provide strength by reinforcing the matrix and toughness by "blunting" or deflecting cracks in CMCs.

Current technology for fiber synthesis is limited in the materials from which fibers can be formed, the quality and diameters of the fibers that can be obtained, and the compatibility with coating materials that could be used to toughen ceramic-ceramic composites. The relatively high cost of oxide fibers available for composite materials makes research and development very expensive.

Recent research [1,2] has shown that fibers can be drawn from containerless melted oxides which are cooled below their melting point (undercooled) to increase melt viscosity. Oxide materials such as mullite ($Al_6Si_2O_{13}$) and yttrium-aluminum garnet or YAG ($Y_3Al_5O_{12}$), which have properties suitable for the structural applications, have been formed into glass fibers by this method. The method is not limited to containerless conditions, since temperature gradients in contained liquids can be designed to provide the required undercooling in the region from which fibers are drawn.

The process of drawing glass fibers from undercooled melts is inexpensive and applicable to a wide range of oxide materials. Accordingly, it would provide an attractive source of materials for high temperature structural applications if two further steps in its development can be successfully completed. The first step is to demonstrate crystallization of the glass fibers into high strength crystalline material. The second is to scale up the fiber pulling and crystallization processes to provide the needed materials. Phases I and II of this research program are concerned primarily with the first and second of these advances in the fiber making technology.

The Phase I research was performed at Containerless Research, Inc. (CRI) in Evanston, Illinois, and at the University of Illinois Urbana-Champaign (UIUC). The overall objective of the work was to establish the scientific basis for synthesis of strong, creep resistant, crystalline oxide fibers for use in high temperature structural applications. The Phase I research focussed on determining process-property relationships for fiber synthesis and crystallization.

The technical activities were to (i) synthesize glass fibers of selected oxide compositions, (ii) characterize the glass fibers, (iii) crystallize the bulk glasses and fibers by controlled heating, and (iv) characterize the crystalline fiber products.

The Statement of Work for the Phase I research is presented in section 2.1 below. The work plan addressed key areas needed to meet the Phase I research objectives and develop the

basis for Phase II and Phase III activities. Fiber processing was performed at CRI, characterization and differential thermal analysis experiments to determine conditions for crystallization from amorphous oxides were performed under the direction of Professor W.M. Kriven at the University of Illinois Urbana-Champaign (UIUC). Research on fiber crystallization was performed jointly at CRI and UIUC.

2.1 Phase I Statement of Work

Discussions with the Air Force led to changes in the emphasis of proposed work which are reflected in the Phase I statement of work given below. However, the title of the project has not been changed. The scope of research on synthesis of crystalline fibers was expanded and work to investigate fiber coatings was eliminated from the project.

The statement of work for the Phase I research has 8 principal tasks:

(1) Prepare and characterize batch quantities of YAG, mullite and other oxide fibers.
(2) Determine optimal conditions for drawing these fibers from undercooled melts.
(3) Measure the tensile strength of the fibers at room temperature.
(4) Characterize the microstructure of the as-spun fibers using TEM and X-ray diffraction.
(5) Determine the appropriate conditions for crystallization of the amorphous fibers.
(6) Thermally convert the fibers into YAG and mullite polycrystalline fibers and establish the optimal conditions for thermal treatment.
(7) Characterize the produced polycrystalline fibers using a variety of appropriate techniques.
(8) Provide mechanical testing, including tensile strength, creep resistance.

All tasks were successfully completed except for parts of tasks 4, 6 and 8. Crystallization rates and behavior were determined at temperatures above and below the optimum temperature conditions and the methods required to obtain optimum heating conditions were determined. These conditions can be readily achieved when long and continuous fibers become available in the Phase II research. The creep measurements on crystallized fibers (task 8) were not performed, since longer fibers and crystallization under optimum conditions to achieve high strength fibers will also be required to perform the creep measurements. The research suggests that long and continuous glass fibers may be converted to single crystal fibers under appropriate heating conditions.

3. EXPERIMENTAL METHODS

The approach to fiber synthesis can be summarized by four principal experimental objectives. They are (i) prepare undercooled liquids from which glass fibers can be drawn with reproducible fiber properties, (ii) draw glass fibers from the undercooled liquids, (iii) measure the kinetics and thermodynamics accompanying the crystallization of bulk glass

beads of the mullite and YAG compositions to obtain temperature-time-transformation (TTT) conditions, and (iv) crystallize the glass fibers under conditions leading to high strength crystalline material. The primary purpose of the materials processing research was to identify the range of conditions in which these operations can be performed to yield high quality fibers.

Previous research has demonstrated that the degree of undercooling and the crystallization behavior of undercooled liquid oxides can vary with the bulk liquid chemical composition, the ambient oxygen partial pressure, and the temperature at which the liquid is preheated before it is undercooled [3,4]. The temperature range over which fiber drawing is possible may be small, since the liquids tend to exhibit a viscosity *vs* temperature behavior characteristic of fragile liquids. The viscosity of the liquid increases slowly as the liquid is undercooled and remains too small to allow fiber drawing, then increases rapidly to permit fiber pulling over a relatively narrow range of temperatures. This range was approximately 50°C for molten $Y_3Al_5O_{12}$ materials.

The cooling rates that resulted when the heating laser beam was blocked in the containerless melt processing experiments were up to 300°C/s at the highest temperatures. Fiber pulling rates were typically 100 cm/s. Thus it was typically possible to obtain 20 cm long fibers under transient conditions where the fiber pulling was initiated at a preselected temperature during the cooling process. In some cases, the fibers were up to 50 cm long. The fibers usually showed large defects near their ends and a central section in which the diameter was uniform. The optimum temperatures for making smooth, uniform diameter and defect-free fibers were determined by inspecting the fibers formed in the experiments.

Fiber pulling during transient cooling of the liquid was necessary because the fiber pulling force was considerably larger than the weight of the levitated liquid drop. Thus, the liquid drop could not be maintained in the levitated condition and it made contact with the surface of the levitator when fiber pulling was initiated. This contact did not greatly increase the cooling rate but it did lead to crystallization of the liquid which terminated the fiber pulling and limited the fiber length.

The formation of bulk glass when the levitated liquid drops were cooled was found to depend on the liquid composition, ambient oxygen partial pressure, and liquid preheating conditions. Since the cooling rate of material pulled from the liquid in the form of a thin fiber was much greater than the bulk cooling rate of the liquid drop, it was possible to make glass fibers from the undercooled liquid whether or not the bulk liquid formed a glass. Fibers could be obtained in all cases where the liquid developed a sufficient viscosity at temperatures above the nucleation temperature for crystallization of the undercooled liquid.

The remainder of this section describes the various experiments performed in the experimental research. It is divided into three principal subsections, on (i) the materials processing experiments, (ii) determination of kinetics and thermodynamic conditions for crystallization from bulk amorphous phase, and (iii) the materials property measurements.

3.1 Processing Experiments

3.1.1 Bulk specimen preparation

Two families of oxide materials were investigated - binary alumina-silica and binary alumina-yttria compositions. Phase diagrams for these two systems are presented in Figure 1 [5-8]. Three different diagrams are given for the alumina-silica system. Emphasis was placed on the mullite and yttrium aluminum garnet (YAG) compositions. The alumina-silica phase diagram shows that mullite can form over a range of alumina:silica compositions near the $Al_6Si_2O_{13}$. The alumina-silica system exhibits considerable metastable behavior. Mullite is reported to melt either congruently or to exhibit peritectic decomposition to a silica-rich and aluminum oxide, at temperatures from 1830-1890°C [5-7]. YAG is formed over a narrow composition range corresponding to $Y_3Al_5O_{12}$ and congruent melting occurs at approximately 1950°C.

Effects of precursor composition on the fiber properties were investigated by using material compositions which bracketed mullite and YAG and by substituting 1 mole% neodymium or erbium oxide for yttrium oxide in the YAG composition. Table I presents the compositions which were used. Spheroidal specimens *ca.* 0.3 cm in diameter were synthesized from high purity oxide precursors using a laser hearth melter [9]. Phase-pure YAG and mullite specimens were made from commercially available crushed single crystal YAG and Kyoritsu mullite [10] and by mixing oxide powders.

3.1.2 Liquid phase processing

Preliminary levitation, melting and cooling experiments were performed to establish levitation conditions. The samples were levitated in a conical nozzle levitator (CNL) [11], and heated and melted with a cw CO_2 laser beam. The levitation gases were pure argon, oxygen, or air. An automatic optical pyrometer recorded the apparent temperature of the top surface of the sample at rates up to 100 Hz. Rapid cooling of the liquid was obtained by blocking the laser heating beam, and either glass formation or nucleation of crystalline materials were observed as the liquid cooled. The heat released upon nucleation, and rapid crystallization of the liquid produced a rapid temperature rise (recalescence) followed by cooling of the solid material. Glass formation resulted in smooth cooling to room temperature without any discontinuity in the measured temperatures.

The process atmosphere and the preheating program at temperatures above the melting point were varied in experiments on different sample materials to determine the effects of these variables on the crystallization and glass forming behavior. Bulk specimens of mullite and YAG composition glass were prepared for use in the differential thermal analysis experiments to determine the crystallization temperatures and rates when the glass samples were slowly heated.

3.1.3 Temperature measurements

The apparent temperatures, T_a, recorded by the optical pyrometer are less than the true specimen temperature due to non-unit spectral emissivity, ϵ_λ, of the materials at the operating wavelength, $\lambda = 0.65\ \mu m$, of the pyrometer. Apparent temperatures are reported and used in this work, since the corrections are not accurately known for the materials. The corrections to obtain true temperature are quite small at higher temperatures. Certain ambiguities in the temperature occur during cooling curves if the specimens become semi-transparent. The relationships between apparent and true temperature are discussed below.

The apparent and true temperature, T, are related by the equation:

$$\frac{1}{T} - \frac{1}{T_a} = \frac{\lambda}{C_2} \ln \epsilon_\lambda \qquad (1)$$

Spectral emissivity values are not available for the materials investigated. However, quite accurate values may be estimated for the high temperature liquids, from Kirchoff's law for opaque materials:

$$\epsilon_\lambda = 1 - r_\lambda \qquad (2)$$

using the normal spectral reflectivity, r_λ, given by:

$$r_\lambda = \frac{(n-1)^2 + k^2}{(n+1)^2 + k^2} \qquad (3)$$

to obtain the normal spectral emissivity.

The refractive indices, n, of the liquids are of similar values to the glasses or crystalline solids of the same composition. The extinction coefficients, k, are typically too small to contribute to the value of r_λ calculated in Equation 3, but sufficient at higher temperatures to make the specimens opaque. We estimate the range of values for n to be 1.5 to 2.0 ($n \approx 1.8$ for liquid aluminum oxide and $n \approx 1.5$ for silica glasses). Thus, at high temperatures, $\epsilon_\lambda \approx 0.89$ to 0.96 and temperature errors due to uncertain emissivity will be rather small (<20K at 2000K and smaller at lower temperatures).

At lower temperatures, when an undercooled liquid approaches the glass transition temperature, the value of k become small enough that the specimen is no longer opaque and the apparent temperature may become much less than the true specimen temperature.

Temperature differences that develop between the surface and interior of specimens during free cooling experiments may also influence the apparent temperature measurements because not all of the emitted light is from the specimen surface.

Somewhat smaller spectral emissivities and larger temperature corrections occur for the solid crystalline materials. For example, the normal spectral emissivity (at $\lambda = 0.65$ μm) of polycrystalline aluminum oxide varies from 0.54 at 1500K to 0.72 at 2000K, while that of liquid aluminum oxide is 0.91 and nearly independent of temperature.

3.1.4 Fiber synthesis

The apparatus for fiber pulling is illustrated in Figure 2. Specimens were levitated in air, oxygen or argon and heated with a continuous-wave CO_2 laser beam. Materials were usually processed in the atmospheres which enabled bulk glass formation in the preliminary experiments. Some fibers were formed from liquids that spontaneously crystallized at a temperature below the fiber drawing temperature. The temperature of the levitated drops was measured with an automatic optical pyrometer whose output was acquired via a LabView computer program.

The fibers were pulled during a transient undercooling process in which the laser beam heating was turned off and the fibers pulled as the liquid cooled. Pulling rates of 100-150 cm/s were used and the cooling rate at the top of the molten oxide droplet was approximately 200°C/s. Stinging and fiber pulling occurred automatically when the measured temperature reached a selected value. The stinger was a 75 μm diameter tungsten wire mounted onto the pulley that operated by a computer-controlled stepper motor. The stinger was injected into the undercooled liquid drop and then rapidly withdrawn to pull the fibers. Experience with the stinger-puller operation led to the selection of an acceleration approximately 10,000 cm/s^2 during injection, withdrawal, and acceleration of the stinger to the final fiber-pulling velocity. Other fiber pulling parameters selected under computer control were the duration, penetration depth, final velocity for fiber pulling and duration of fiber pulling.

3.1.5 Fiber crystallization

Crystallization rates were first determined by heating bulk glass samples in DTA experiments and by measuring the rate of crystallization when crystals spontaneously nucleated and grew in undercooled bulk liquid samples. Based on these results, two methods, using slow and fast heating, were used to crystallize the glass fibers. The first method was to heat the fibers in a furnace by increasing the furnace temperature at rates of 10°C/min to preselected maximum temperatures of 1000-1200°C, hold the specimen at the maximum temperature for 1-4 hours, and then cool it at a rate of approximately 20°C/min. The second, fast heating method, was to rapidly insert the fibers into a furnace that was already at the temperature of interest. Fast crystallization was performed at temperatures of 1100, 1200, 1300, and 1400°C, with residence times in the furnace of 5, 15, and 30 s.

3.2 Determination of Thermodynamic and Kinetic Conditions for Crystallization from Bulk Amorphous Phase

Non-isothermal differential thermal analysis (DTA) was performed on glassy mullite and glassy yttrium aluminum garnet (YAG) specimens to examine the crystallization kinetics of each material. The objective was to determine the activation energy for crystallization (E) and the frequency factor (ν) and use these parameters to calculate crystallization as a function of time and temperature. The kinetic model of Bansal and Doremus [14] was used to determine the kinetic parameters.

Spheroidal glass specimens of the Kyoritsu mullite and YAG compositions (with 1 mol % Nd_2O_3 substituted for Y_2O_3) were made by containerless cooling of melts. The glass was ground to a fine powder in an alumina mortar and pestle. Weighed portions of approximately 30 mg of the crushed glass were placed in alumina crucibles for DTA analysis (Netzsch STA 409 Simultaneous Thermal Analyzer, Selb, Germany).

Six DTA runs were performed on each material. The specimens were initially heated up to 500°C at a rate of 10°C/min for each run. Above that temperature, different heating rates of 2.5, 5.0, 10.0, 20.0, 30.0 and 40.0 °C/min were used in the six experiments for each material. The data was collected digitally and subsequently examined to determine the peak temperature and peak width at half-maximum for each exotherm.

3.3 Materials Property Measurements

The fibers pulled from undercooled melts were first inspected with a 5X hand lens and their length was measured. The fibers were attached to a card which was labeled for reference purposes and retained for further inspection and property measurement experiments.

In the search for optimum fiber growing conditions, many fibers were formed that showed easily observed defects, large variations in fiber diameter and short opaque regions that were possibly caused by the presence of crystalline material. These fibers were not evaluated further.

Conditions were found that resulted in long defect-free sections of fiber with uniform diameters, smooth surfaces and no visible changes in appearance along the fiber. However, even the best fibers had defects near their ends, since the fiber pulling occurred in a transient process in which significant changes in the liquid temperature occurred as the fiber was pulled. The long fiber sections which showed no visible defects were viewed at 175X under a video microscope. Test specimens were cut from these sections for mechanical property testing, crystallization experiments and further examination by SEM and TEM.

3.3.1 Glass fiber inspection

Preliminary tensile tests showed large variations in the mechanical properties of fibers with the same composition. The variations were traced to the presence flaws which sometimes occur along the length of the fiber. Fiber inspection was developed to select fibers for mechanical testing and to help determine fiber pulling conditions that yield uniform diameter defect-free fibers.

The fiber inspection system is illustrated in figure 3. The fibers were mounted on a computer-controlled translation stage and arranged so that the fiber lay in the focal plane of a 175X video microscope. The fiber was translated under the field of view of the microscope and a video record was made of the image for the full length of the fiber. The video record was reviewed to select sections of the fiber for property testing and crystallization experiments.

Four video microscope images of glass fibers are given in Figure 4. Mullite-composition fibers are on the left and YAG-composition, with 1 mol % Nd_2O_3 substituted for Y_2O_3 in the material, are on the right side of the figure. Defects appeared in the fibers as changes in the diameter (top of the figure). The defects were generally smooth changes over a length of several diameters for mullite or small nodules for YAG-compositions. The bottom part of the figure shows typical defect-free fibers selected for property measurements and crystallization experiments.

3.3.2 Mechanical testing

Mechanical testing was performed at the University of Illinois Urbana-Champaign (UIUC). The fiber strength was measured using a fixture developed at UIUC for high-modulus single-filament materials. The fiber diameters were 4-41 μm, the gauge length was fixed at 23 mm, or 500-6,000 times the fiber diameter.

Test fibers were bonded into a specially designed frame with "M-Bond" epoxy adhesive. The measurement technique and interpretation was consistent with ASTM standard D3379-75. Tests were performed in an Instron 1205 tensile testing machine operated under computer control. Fibers were pulled at a constant strain rate of 5 μm/s. A high sensitivity load cell equipped with a fully digitized controller was used to measure load.

A computer was used to record the load and displacement as a function of time. Broken fibers were examined by optical microscopy to determine the cross section so that stress could be determined.

3.3.3 Materials characterization

Microstructural characterization included scanning electron microscopy. Prior electron diffraction measurements have identified crystalline mullite as the material formed by heat

treating of the mullite-composition glass fibers [2]. X-ray diffraction was employed to show that crystalline YAG was the product formed from glassy YAG in the DTA experiments.

4. RESEARCH RESULTS

4.1 Behavior of Undercooled Melts

Figures 5 and 6 present cooling curves under containerless conditions in the CNL apparatus for YAG- and mullite-composition materials, respectively. Each figure shows a sequence of free cooling events for the same specimen when the heating laser was turned off and the melt cooled in the argon levitation gas used for these experiments. The time between subsequent cooling curves was approximately 1 minute and the time intervals were changed to illustrate the sequence of curves in a single figure. The results are typical of the behavior observed in undercooling experiments on a new sample under containerless conditions.

Each cooling curve shows an initial temperature just below 2000K, which is the "railed" output of the optical pyrometer on its most sensitive scale. Higher temperatures can be measured on a less sensitive scale, but the purpose in these experiments was to have high sensitivity for fast measurement of lower temperatures. The actual initial temperatures exceeded the material melting temperatures of approximately 2250K for YAG and 2130K for mullite.

The results for YAG compositions (Figure 5) show a rapid temperature decrease followed by recalescence of the specimen - an increase of temperature due to the heat released by rapid crystallization of the undercooled liquid, and then followed by a rapid temperature decrease of the solid. The nucleation temperature, T_N, is the minimum temperature prior to recalescence and the recalescence temperature, T_R, is the maximum temperature following crystallization. It can be seen that the values of T_N are initially in the range 1600-1700K and then decrease and become reproducible at approximately 1360-1400K. These differences were attributed to the occurrence of two different solidification paths. The first, releases less heat and results in a metastable mixture of yttrium-aluminum perovskite (YAP, $YAlO_3$) and aluminum oxide at the metastable eutectic temperature of this mixture. The second releases more heat to form the stable equilibrium product, yttrium-aluminum garnet (YAG, $Y_3Al_5O_{12}$) with the same composition as the bulk liquid.

The results for mullite composition melts (figure 6) also show variations in undercooling behavior. Deep undercooling to about 900K below the melting point is seen in the first curve, followed by glass formation in the second curve. Subsequent cooling curves showed nucleation at 1500-1600K. Continued processing of mullite compositions in argon gas led to reproducible nucleation and recalescence results.

The cooling curves for a mullite-composition melt were obtained to illustrate the variations in behavior that occur as the period of melt processing increases. Accordingly, the first two

cooling curves were obtained sooner after initial melting that were the cooling curves on other samples. The extremely deep undercooling shown in the first curve of Figure 6 was not observed in any other experiments with the mullite composition melts. Also, glass formation, shown in the second curve was rarely observed when the mullite samples were heated and melted in a flow of argon gas. Nucleation and recalescence did not occur, i.e., the specimens formed glass, when molten mullite was cooled in air or oxygen. The variations in behavior shown in figure 6 were therefore attributed to slight changes in the oxygen content of the melt with process time during the sequence of cooling experiments.

Glass formation never occurred from YAG composition specimens formed from crushed single crystal YAG material, but synthetic YAG compositions formed from mixtures of Al_2O_3 and Y_2O_3 powders sometimes formed glass when the melt was cooled in argon gas. It was found that addition of 1% excess alumina to the YAG composition resulted in reproducible glass formation. The variations in crystallization behavior of the synthetic YAG compositions was attributed to small composition variations in the material. Reproducible bulk glass formation was also observed for YAG compositions with (i) 1 mol % Nd_2O_3 substituted for Y_2O_3, and (ii) 1 mol % Er_2O_3 substituted for Y_2O_3 and a 1 mole % excess of Al_2O_3 added to the sample. The material with 76 mol % Al_2O_3 and 24 mol % Y_2O_3 (near to the eutectic composition, (see Figure 1) always crystallized upon undercooling of the melt.

Figure 7 illustrates, with an expanded time scale, the first and last cooling curve from Figure 5 for YAG-composition melts. A temperature arrest followed by a slow cooling rate is observed in the first curve, for approximately 2.5 sec subsequent to the recalescence event. nucleation of is observed in the first curve at this temperature. However, no temperature arrest or reduced cooling rate was found for YAG composition melts that undercooled to 1360-1400K. These melts were hypercooled, i.e., complete solidification of the melt did not release sufficient heat to achieve a solid/liquid equilibrium temperature, so that the solid cooled rapidly and immediately after the recalescence peak temperature was reached.

It has been shown [12,13] that a mixture of $YAlO_3$ and Al_2O_3 is formed by undercooled YAG-composition melts that nucleate at temperatures near 1600K. The temperature arrest observed for these melts must then correspond to a metastable eutectic between $YAlO_3$ and Al_2O_3, whose temperature will be less than the equilibrium YAG-Al_2O_3 eutectic temperature of 2093K.

Figure 8 shows the cooling curves for mullite compositions from Figure 6 for which recalescence occurred, with an expanded time scale. These results were obtained on samples of Kyoritsu mullite, whose composition is precisely 40 mol % SiO_2 and 60 mol % Al_2O_3. It is seen that recalescence occurs by a rapid temperature rise to 1750-1800K followed by a slower increase to over 1900K and cooling of the solid. The abrupt change in heating rate during recalescence may result from a crossing of the phase boundary of the mullite phase, which in Figure 1 (bottom left part) is shown to exceed 40 mol% SiO_2 at temperatures above 1600°C.

4.1.1 Crystallization rates of undercooled melts

The recalescence events for the YAG-composition melt from Figures 5 are shown with an expanded time scale in Figure 7. These results, and the mullite data in Figure 6 allow estimates of the crystallization rates in the undercooled liquids. These data were obtained with the CNL apparatus, in which the top part of the specimen exhibits a smaller heat transfer coefficient than the bottom part, so that nucleation occurs at the bottom and the crystals propagate to the top surface where temperatures are measured. The recalescence rise time can thus be taken equal to the time interval required for crystals to propagate a distance less than the specimen diameter (3 mm) but greater than the radius of the spot observed with the optical pyrometer (ca. 0.7 mm). The deeply undercooled YAG compositions (bottom part of Figure 7) show a rise from the nucleation temperature to the recalescence temperature in 50 ms and the velocity of the crystal growth is estimated to be:

$$u(\text{YAG crystallization}) = 1.4 \text{ to } 6 \text{ cm/s} \quad \text{at } T = 1400 - 1900\text{K} \tag{4}$$

Similarly, from the first three and fifth curve in Figure 5, where the rise time is 100 ms:

$$u(\text{YAP + alumina crystallization}) = 0.7 \text{ to } 3 \text{ cm/s} \quad \text{at } T = 1700 - 1900\text{K} \tag{5}$$

The rapid initial temperature rise during recalescence of molten mullite (Figure 6) occurred in 20-80 ms, and the later, slower rise time was 120-200 ms. The initial rise is attributed to congruent solidification of the liquid:

$$u(\text{congruent crystallization of mullite}) = 3.5 - 15 \text{ cm/s} \quad \text{at } T = 1500\text{-}1800\text{K} \tag{6}$$

Further experiments will be required to explain the reduced crystallization rate in the latter part of the recalescence events for mullite. It is possible that the reduced crystallization rate occurs because crystal growth from the liquid becomes incongruent at temperatures where the 40:60 SiO_2:Al_2O_3 composition is outside the mullite phase field. If this is correct, experiments with compositions slightly greater than 60 mol % Al_2O_3 should yield congruent solidification and more rapid crystallization for the entire recalescence event.

4.2 Fiber Synthesis

Glass fibers were synthesized by pulling from undercooled melts [1,2]. The first stage of the work was to investigate the effects of precursor compositions and process variables on the properties of the glass fibers. Fibers used for the crystallization research were then made using pulling conditions selected to obtain uniform fiber properties. This following sections describe the fiber synthesis research.

4.2.1 Fiber pulling research

Process conditions for bulk glass formation under containerless conditions also enable fibers to be pulled from the undercooled melt. Conditions which favor bulk glass formation were determined in preliminary experiments. Investigation of fiber pulling from binary yttria-alumina compositions revealed subtle composition-dependent effects. The first indication of these effects was that some specimens from a batch could easily be pulled into fiber while others could not. The differences were attributed to small compositional inhomogeneities which occurred in the specimens prepared by hearth melting mixed oxide powders. The hearth melting procedure was modified and specimens were made from small quantities of powder which could be completely melted to ensure homogenization. The following guidelines were established for processing materials for fiber pulling:

1. Levitated material needs to be completely melted so that no residual solid nuclei remain in the liquid. This was accomplished by superheating the levitated drops 50-100° above their equilibrium melting point.

2. Processing in oxygen favors glass formation in alumina-silica materials.

3. Processing in argon favors glass formation in alumina-yttria materials.

4. Adding 1% excess alumina or substituting 1% neodymium oxide for yttrium oxide in the YAG-composition enhanced glass formation. Bulk glass was not formed from phase-pure YAG.

High quality mullite-composition glass fibers were pulled from melts in the apparent temperature range from 1760-1775K or approximately 350K of undercooling. YAG-composition glass fibers were pulled in the apparent temperature range from 1600-1680K or approximately 600K of undercooling. Compositions containing 1 mole% excess alumina, or 1 mole% neodymium oxide substituted for yttrium oxide could easily be pulled into fibers. Fibers of a few mm length were occasionally obtained from phase-pure stoichiometric YAG melts. Glass fibers were pulled from the 76 mol % alumina - 24 mole% yttria compositions even though these materials did not form bulk glasses.

4.2.2 Fiber synthesis for testing and crystallization research

The YAG composition containing 1% neodymium oxide substituted for yttrium oxide was selected for fiber testing and crystallization experiments. This composition has the same rare-earth:aluminum ratio as YAG and is known to form homogeneous single crystals used in Nd-YAG lasers. Crystallization of the glass with this composition can proceed without rejection of "excess" alumina.

Mullite composition glass fibers prepared for fiber testing and crystallization experiments were formed from precisely 40:60 (mol %) SiO_2:Al_2O_3 Kyoritsu mullite (3 Al_2O_3 2 SiO_2) and pulled in pure oxygen gas.

Figure 9 illustrates the cooling curves observed in preprocessing and fiber synthesis experiments. The top part shows cooling curves resulting in bulk glass formation for mullite- and YAG-composition melts with (i) 1 mol % Nd substituted for Y and (ii) 1 mol % Er substituted for Y with and excess of 1 mol % Al_2O_3. The bottom part shows the cooling curves during fiber pulling, with arrows marking the apparent temperatures at which the fiber pulling was initiated. The fiber pulling force was sufficient to pull the levitated specimen into contact with the conical nozzle levitator, and this contact resulted in heterogeneous nucleation of crystals and recalescence of the specimen. It can be seen in the figure that recalescence occurred within 0.5 seconds after fiber pulling was initiated. The fiber pulling rate was typically 100 cm/s and fibers up to 50 cm long were obtained.

4.3 Fiber Characterization

4.3.1 Mechanical testing

Figure 10 shows a typical stress *vs* strain plot for a mullite-composition glass fiber and Figure 11 shows tensile strengths of binary alumina-silica fibers with alumina concentrations from 50-65 mol % alumina.

Figure 12 shows a typical stress *vs* strain plot for a YAG-composition fiber with 1 mol % Nd substituted for Y. Fracture strength measurements for several of these fibers are given in Table II.

4.3.2 Scanning electron micrographs of mullite and YAG composition glass fibers

Figures 13-16 show scanning electron micrographs of the surface and fracture sections of mullite and YAG glass fibers. The YAG fiber shown was obtained in a preliminary experiment and was evidently of a composition slightly rich in aluminum oxide.

4.4 Thermodynamic and Kinetic Conditions for Crystallization from Bulk Amorphous Phase

Figures 17 and 18 present the DTA measurements for glassy YAG and glassy mullite, respectively. For heating rates from 2.5-40°C/min, the crystallization exotherms peak at 924-976°C for YAG and at 956-1014°C for mullite.

The six sets of data for each material are shown on single plots in Figure 19, after normalizing the measurements to a common baseline temperature difference. It can be seen that the YAG data (bottom part of Figure 19) exhibit two peaks at lower heating rates and

temperatures, with the second peak dominating at higher temperatures. It is possible that two crystallization paths occur, as was observed for the undercooled melts.

4.4.1 Data analysis

The kinetics of crystallization can be described by the Johnson-Mehl-Avrami (JMA) equation [15]:

$$x = 1\text{-}\exp[-(kt)^n] \tag{7}$$

where:

x = fraction of material converted to the new phase
k = reaction rate constant, s^{-1}
t = time
n = Avrami exponent which depends on the geometry of the crystallization mechanism.

The JMA equation can be used to present isothermal phase transformations by plotting the percentage transformed as a function of time and temperature. These plots are called TTT diagrams (transformation, time, temperature) [15] and in the case of crystallization, provide important information on how the rate of crystallization varies with time and temperature. This information is critical in order to effectively design experiments and processes for the crystallization of amorphous fibers. However, in order to use this equation and develop TTT diagrams, the reaction rate constant and the Avrami exponent must be experimentally determined.

The reaction rate constant is not a constant, per se, but is a function of temperature, activation energy and frequency factor. The equation for the reaction rate constant, k, can be described by an Arrhenius equation:

$$k = \nu\exp(-E/RT) \tag{8}$$

where:

ν = Frequency factor, s^{-1}
E = Activation Energy, KJ/mole
R = Gas constant, J/(mole K)
T = Temperature, K

Thus, in order to calculate the reaction rate constant, the activation energy and the frequency factor must be determined. These parameters may be determined experimentally using non-isothermal differential thermal analysis (DTA) and evaluating the results using a kinetic model derived by Bansal and Doremus [14,16,17]. The result of their derivation is a slope-intercept

equation based on the peak temperatures for crystallization exotherms measured at different heating rates.

$$\ln[T_p^2/\alpha] = E/R(1/T_p) + \ln(E/R) - \ln(\nu) \quad (9)$$

where:

E = Activation Energy, KJ/mole
T_p = Peak temp on DTA curve, K
α = Heat up rate, °C/min
R = Gas constant, J/(mole K)
ν = Frequency factor, s^{-1}
m = slope
b = y intercept

This data can be plotted in a line, and the activation energy can be calculated from the slope and the frequency factor from the y-intercept. The following equations apply:

$$y = mx + b \quad (10)$$

where:

$$y = \ln[T_p^2/\alpha] \quad (11)$$
$$x = 1/T_p \quad (12)$$
$$m = E/R; \quad \text{or } E = mR \quad (13)$$
$$b = \ln(E/R) - \ln(\nu); \quad \text{or } \nu = (E/R)\exp(-b) \quad (14)$$

The Avrami exponent can be calculated using an expression developed by Augis and Bennett [14]:

$$n = (2.5/\Delta T_{FWHM})^* T_p^2/(E/R) \quad (15)$$

where:

ΔT_{FWHM} = The width of the exotherm maxima at half of its maximum height (Full Width Half Maximum)

Thus, by running several DTA experiments at different heating rates and measuring the peak temperature of each exotherm, the activation energy and frequency factor can be calculated (using linear regression) from a plot of Equation 9. Subsequently, the reaction rate constant can be calculated from E and ν using Equation 8, and the Avrami exponent can be calculated using Equation 15. Consequently, all of the necessary parameters for using the JMA equation and calculating TTT diagrams can be determined from non-isothermal DTA experiments.

4.4.2 Results

Tabulated results for the activation energy, frequency factor (or attempt frequency) and the Avrami exponent are shown in Table III.

Plots of the raw data showing DTA traces for both materials at each heating rate are included in the appendix. The above data was used to generate graphs of $\ln(T_p^2/\alpha)$ vs $1/T_p$ (using Equation 9) and to calculate the activation energy and frequency factor using Equations 10-14). These plots for both glassy mullite and YAG resulted in relatively straight lines with correlation coefficients (as determined by linear regression) of 0.991 and 0.985 respectively. These graphs are also included in the appendix. Based on this information, the reaction rate constant was calculated as a function of temperature. A value of 1 was chosen for the Avrami exponent, n, which is characteristic of one dimensional growth of a constant number of nuclei.[2] This value was chosen so as to model a planar crystal growth front for single crystal growth of amorphous fibers. These parameters (E, ν, k, and n) were used in the JMA equation to plot the percentage of crystallization as a function of time at various temperatures. Additionally, TTT curves were also generated using the JMA equation by plotting the temperature required to achieve a specified percentage of crystallization (e.g. 1% and 99%) as a function of time. These diagrams are given in Figures 20 and 21.

4.4.3 Discussion of results

As noted previously, the activation energy computed for mullite crystallization in this study was relatively high. In a paper by Bansal and Hyatt [17], the activation energy for mullite crystallization from a BaO-Al_2O_3-SiO_2 glass system was 553 KJ/mole. The reason for this may be due to the difference in composition of the two systems. In this study, pure mullite was examined whereas in the study by Bansal, there was the addition of BaO which may effect the diffusional and kinetic mechanisms of crystallization. Another possible explanation may be that in the glass system Bansal examined, the crystallization exotherms occurred at higher temperatures than in this study (20 - 50°C higher). One of the assumptions behind the kinetic model of Bansal and Doremus is that the activation energy and frequency factor are independent of temperature [14]. This is an approximation which is only valid over narrow ranges of temperature. In fact, E and ν are a function of temperature and can vary significantly over wide temperature ranges. For example, in another glass system, Bansal reported significant differences in the activation energy for crystallization at different temperatures [16].

Another feature of the mullite kinetic data is that the frequency factor (or attempt frequency) is very high (13 orders of magnitude higher than that for YAG). Another assumption used in the kinetic model by Bansal and Doremus is that the rate of reaction is a maximum at the exothermic peak. This is valid for compensated differential scanning calorimetry (DSC, which has a limited temperature range) but not for DTA. In DTA, the peak corresponds to the point at which the temperature difference between the sample and the reference is zero [17]. However, "So long as a consistent point is chosen, e.g., peak temperature, onset

temperature, etc., to represent a given process in a series of DTA traces recorded at different scan rates, activation energies in agreement with the DSC results would be obtained [17]. Once of the consequences is that though accurate values of the activation energy can be obtained from the slope of Equation 9, the value for the attempt frequency (based on the y-intercept) will depend on the representative point chosen. Additionally, Bansal reported that the value of the attempt frequency was sensitive to experimental variations in processes with high activation energies [16].

The values for activation energy and attempt frequency for YAG were closer to the values reported for other materials in the literature. It was observed that at low heating rates (2.5, 5.0, and 10.0 °C/min), two different exothermic events occurred. This could indicate an additional polymorphic phase transformation from a metastable state such as two crystallization events, one from pre-existent nuclei and the other from newly formed nuclei, or the formation of metastable phases and their subsequent conversion to a more stable phase. Further experimental analysis is required to determine what this other event is. Kinetic analysis was based on the first exotherm. At higher heating rates, it was not possible to distinguish between the two different exothermic events.

The Avrami exponents calculated for both glassy mullite and glassy YAG show wide variations. The expected result was a consistent value close to 3 (assuming growth of a constant number of nuclei) for each DTA run. The variation in n indicates that the number of nuclei probably changed with time and temperature and that the rate of nucleation was not constant. Isothermal DTA or DSC methods can be used to obtain more accurate values for the Avrami exponent and the attempt frequency.

The most significant information generated from this study is found in the TTT diagrams and the percentage of crystallization as a function of time for various temperatures plots. This information was calculated using the JMA equation and the values for E and ν found from the DTA experiments. (As previously stated, a value of 1 was chosen for the Avrami exponent). Selected results are shown in Table IV.

These results show that crystallization is very sensitive to temperature. For the case of mullite, even though it has a much higher activation energy for crystallization than YAG, the TTT diagram results show the dominating influence of the attempt frequency as the temperature increases, thus resulting in faster crystallization rates at elevated temperatures.

This information can be directly applied to designing experiments and techniques for the crystallization of amorphous fibers. For example assume that there is a 15 μm diameter fiber with a 5 μm wide crystal growth front that is being crystallized into a single crystal by being pulled through a furnace at a fixed temperature of 1100°C. At that temperature, it could be pulled at a rate of 0.21 mm/s (5μm/0.024s = 0.21 mm/sec) while maintaining only the growth front in the hot zone. That equates to a rate of 0.75 m/hr for producing single crystal mullite fibers. For a similar amorphous YAG fiber in an 1100°C furnace, it could be pulled at a rate of 0.125 mm/sec which equates to .45 m/hr of single crystal YAG. At a

temperature of 1200°C, a similar mullite fiber could be crystallized at a rate of 62.5 mm/s (225m/hr) and an amorphous YAG fiber could be crystallized at a rate of 5.55 mm/s (20 m/hr).

It is important to note that these are tentative values subject to further experimental verification and refinement of the kinetic variables calculated through this study. However, as the data shows, the rate of crystallization is highly temperature dependent and even higher production rates would be possible at elevated temperatures.

4.4.4 Conclusions

The prospect for efficient and cost-effective mass production of crystallized amorphous fibers looks very promising. It appears that relatively fast rates of crystallization are theoretically possible. Some critical factors necessary for the realization of this potential is the precise in-situ control of the temperature and the crystal growth front so as to ensure single crystal growth.

As noted in the discussion section, there is some question as to the accuracy of the attempt frequency and the Avrami exponent calculated from this set of experiments. Further thermal analysis using isothermal DTA or DSC methods are required in order to obtain more accurate information on these values and to gain additional understanding into the crystallization mechanism of these materials. Additionally, such experiments will also provide information on the heat capacities and heats of crystallization for these materials. These are important parameters to know since crystallization is an exothermic process and controlled, uniform heat evolution at the amorphous/crystal interface is necessary for the development of a uniform interface and the prevention of dendritic growth.

4.5 Crystallization of Glass Fibers

The first set of fiber crystallization experiments was performed at heating rates from 2.5 to 40°C/min, using the same methods as in the DTA experiments. Heating conditions for the crystallized fibers are given in Table V. Prior electron diffraction measurements have identified crystalline mullite as the material formed by heat treating of the mullite-composition glass fibers [2]. X-ray diffraction showed that crystalline YAG was the product formed from glassy YAG in the DTA experiments and it was assumed that crystalline YAG was also the product of glassy YAG fiber crystallization.

The second set of crystallization experiments was designed to obtain much larger heating rates of several 100°C/sec. One end of each fiber was cemented to the end of a long alumina rod, and the fiber was inserted into a furnace at the final process temperature. Insertion time was approximately 1 second, and heat transfer to the fiber was sufficient to heat it to the final temperature in less than 1 second. Process temperatures were 1100-1400°C and the fibers were held in the furnace for 5, 15, or 30 sec. Figures 22 and 23 show scanning electron micrographs of the surface and fracture sections of YAG fibers

processed at each temperature and held at temperature for the minimum or maximum period. Similar results for mullite are given in Figures 24 and 25.

5. DISCUSSION

5.1 Fragile Behavior of Undercooled Molten Ceramics

Figure 26 presents a summary by Angell [18] of fragile and strong behavior in various glass-forming systems, in a plot of melt viscosities as a function of reciprocal temperature, normalized by the glass transition temperature. Strong behavior, e.g., by liquid SiO_2 is exhibited by an Arrhenian behavior in which log (viscosity) is proportional to reciprocal temperature over the full temperature range. Fragile behavior is observed as a large departure from Arrhenian behavior. It is noted that the liquids shown to be highly fragile are not liquid ceramic materials but rather are low melting compounds such as chlorobenzene, fluorotoluene, o-terphenyl, ethanol, glycerol, and others.

The present work provides the first results showing highly fragile behavior by a ceramic liquid. The evidence for this fragile behavior by undercooled molten YAG compositions is given below.

Figure 27 plots the viscosity of molten YAG *vs* reciprocal temperature from four different sources. The point at $1/T = 0$ is the observation by Angel [18] that liquids exhibit a common intercept at approximately 10^{-4} poise in the plot of log (viscosity) vs 1/T. The point at 10^{13} poise is at the glass transition temperature of 1150°C by Aasland and McMillan [19]. Viscosity measurements in the liquid above the melting point are reported by Fratello and Brandle [20] are also shown in the Figure. The final data are those obtained from our fiber-pulling experiments, where the viscosity is taken to be within the glass working range for temperatures where it was possible to pull fibers from the melt. It can be seen that the lines connecting these viscosity data show highly fragile behavior.

It is evident that fragile behavior occurs in many other ceramic melts, including all of the melts for which we have been able to pull fibers from undercooled liquid. The temperature range in which fibers may be pulled from the undercooled melts is always observed to be quite narrow, showing a large variation of viscosity with temperature. However, at temperatures above the melting point, the melts are fluid and exhibit a relatively small variation of viscosity with temperature. Systems in which we have observed this behavior and pulled fibers from undercooled melts include high alumina compositions in the silica-alumina system, and the calcia-alumina, magnesia-silica, alumina-lanthana, and alumina-lithia-silica systems.

5.2 Crystallization in the Rapid Heating Experiments

The DTA experiments performed at the slowest heating rates of 2.5°C/min showed the onset of bulk glass crystallization at approximately 960°C for mullite-composition glass and at 915°C for YAG-composition glass. The data showed that the onset temperature increased with the heating rate and the rate of crystallization increased with temperature. The analysis predicted crystallization rates at 1200°C to be on the order of 6 cm/s for glassy mullite and 0.5 cm/s for glassy YAG.

Rates of crystallization of the bulk phase determined by observing recalescence of undercooled melts were 3.5 - 15 cm/s at T = 1500-1800K for the mullite composition and 1.4 to 6 cm/s at T = 1400 - 1900K for molten YAG. Further the experiments with undercooled melts also showed that nucleation of crystals in the melt occurs at a negligible rate at temperatures above 1500K for the mullite composition and above 1400K for the YAG-composition. Bulk glass samples were formed from Nd-doped YAG composition liquids at cooling rates of 120°C/s.

These observations led us to the hypothesis that rapid heating of the glass fibers to temperatures of 1200°C would greatly reduce the number of crystals that nucleate during the heating process and greatly increase the crystallization rate, leading to coarse-grained crystalline fibers. The results that motivated the rapid heating experiments and the temperatures to which the fibers were heated are summarized in Figure 28. These fiber heating experiments verified the hypothesis and showed that the glass fibers exhibit the high crystallization rates that were measured for undercooled liquids and predicted for the bulk glass materials. The results also suggest a method, discussed below and in the following Section, by which single crystal fibers may be obtained by controlled crystallization of the glass fiber precursor materials.

Figure 28 shows cooling curves for pure molten YAG and for Nd-doped YAG. Crystal nucleation always occurred in pure molten YAG, typically at a nucleation temperature, T_N in the range 1360-1400K, resulting in a temperature increase of approximately 500K due to the heat released by rapid crystallization of the undercooled liquid. The cooling curve for Nd-doped YAG resulted in glass formation and provides an upper bound on the critical cooling rate for glass formation. These cooling curves suggest that a heating rate of approximately 120°C can be used to form and undercooled liquid from the glass, without encountering nucleation and crystallization during the heating process. A fast heating process would then be able to access the temperatures above T_N, at which spontaneous nucleation of crystals does not occur in the liquid, and extremely rapid growth occurs for crystals that may already be present or by growth initiated by heterogeneous nucleation.

Figure 28 also shows the temperature ranges for (i) fiber pulling, (ii) nucleation of crystals in the undercooled liquid, and (iii) "DTA response", which is the temperature interval where crystallization occurred in bulk glass heated at 2.5-40°C/minute. These results allowed the design of fast heating experiments. The upper limit on temperature will be in the fiber

pulling range (*ca.* 1600K), above which the liquid viscosity becomes small, allowing shape changes of the molten fiber. This is also the upper limit on fibers heated under moderate tensile forces. The lower limit on preheating of glass fibers is below the DTA response range, *i.e.*, below about 1100K.

Now consider the following circumstance. A glass fiber is held in a furnace at a temperature below 1100K so that it will not crystallize, and crystallization of the fiber is induced in a small region along its length by slightly greater heating at that point. For example, a pulsed radiant heat source could be focussed onto a small section of the fiber to initiate crystallization. If the quotient of the crystal growth rate and the fiber heat transfer coefficient is large enough, propagation of the crystal will yield a temperature rise at the growth front that is approximately equal to the temperature change upon recalescence of the undercooled melt, *i.e.*, 500°C (c.f. the YAG recalescence result in Figure 28). At the same time, a thin boundary layer of glass near the crystal/glass interface will also be heated to high temperature by heat transfer from the hot crystalline material, allowing the rapid crystal growth to occur; the process will be self-sustaining once it is initiated. This experiment was not possible in the current work, but it was possible to rapidly heat the glass fibers to high temperatures by inserting them into a preheated furnace. The lines shown on the left side of Figure 28 show the crystallization temperatures that were thus investigated. The scanning electron micrographs in Figures 22 and 23 show that large crystals were rapidly formed in these experiments, which verified that rapid heating can be used to increase the quotient of the crystal growth and the nucleation rate, to form large crystals directly from the melt. If the preferred direction of crystal growth can be aligned with the fiber axis, single crystal fibers may be obtained, by a very rapid and economical process.

5.3 Single Crystal Fibers by Crystallization of Glass Fibers

There are several results in the present work that lead to the hypothesis that single crystal fibers may be formed from the glass fibers. These results include:

1. DTA results discussed in Section 4.4.
2. Demonstration of fragile behavior in undercooled YAG- and mullite-composition melts.
3. The ability to avoid nucleation of crystals in fibers rapidly heated to temperatures above the nucleation temperature.
4. The fast growth, at several cm/s of crystals from the undercooled liquid, directly demonstrated in undercooling experiments and also predicted by the DTA analysis.
5. The heat release by rapid crystallization is sufficient to rapidly heat glass through the temperature range where nucleation of crystals occurs.
6. Crystallization of YAG-composition glass to form dense crystal grains with dimensions of approximately 10 μm shown in the rapid heating experiments.
7. The ability of fibers heated to temperatures where rapid crystallization occurs to maintain their shape under stresses in excess of the fiber pulling force.

These results suggest that conditions for crystallization of the fibers may be found that will lead to continuous and rapid conversion into single crystal fibers. There are additional results discussed below that suggest the issues that need to be understood and areas for further research towards single crystal fiber synthesis.

Considerable differences were observed in the microstructure of fibers crystallized under different heating conditions. All fibers crystallized at slow heating rates (up to 40°C/min) were fine grained. Judging by the DTA results, these fibers were completely crystallized at temperatures below about 1030°C for mullite and about 980°C for YAG. The occurrence of fine grained material is understood, since crystal growth is slow at these temperature leading to the nucleation of multiple grains before any of them become large.

The grain size differences between YAG- and mullite-composition glass fibers crystallized at high heating rates is not so easily explained. It is possible that the upper temperature limit for fast heating experiments (1400°C) was sufficient to obtain coarse grained YAG but not sufficient to obtain coarse grained mullite. This idea arises from the fact that liquid mullite is more viscous than liquid YAG, at equal temperatures: the fiber pulling temperature for mullite was 100-150°C greater than for YAG. Additional experiments need to be performed on mullite-composition fibers at temperatures up to about 1600°C.

Undercooled melts have not been subject to detailed investigations that would provide a wide property and phenomenological basis for mechanistic discussion. Therefore, a discussion of the mechanistic effects responsible for differences in the crystallization of mullite and YAG are necessarily speculative. Some discussion is warranted, since it helps to indicate areas for further inquiry that would be particularly relevant to fiber crystallization issues. One such area involves metastable behavior of undercooled melts. Metastability is well known in the alumina-silica system and several metastable phase boundaries are shown as dashed lines in one of the alumina-silica phase diagrams of Figure 1. Phase separation can occur in undercooled melts, to yield two liquid phases of slightly different composition. Phase separation of deeply undercooled yttria-alumina melts was recently reported [19], at compositions richer in alumina than the YAG composition. Even though the cooling rates in fiber pulling experiments may be too fast to permit separation into distinct liquid phases, the tendency towards phase separation could result in modulations in the glass fiber composition. Thus metastable and phase separation processes may provide a mechanism to explain the diameter variations in some of the fibers pulled from the melts. The appearance of rapid and slower rise times in the mullite recalescence curves, and the differences in microstructure of the crystallized YAG and mullite fibers could also result.

A second area in which there is mechanistic evidence relevant to crystallization of undercooled melts is in the effect of the ambient oxygen partial pressure on (i) glass formation and (ii) microstructure of crystallized materials. The first of these was demonstrated in the present work, where YAG-compositions (doped with Nd or slightly enriched in Al_2O_3 formed glass when cooled in argon and crystallized spontaneously when cooled in air or oxygen. Similarly, mullite compositions formed glass in air or oxygen and

crystallized when cooled in argon. The effects of the oxygen partial pressure on the microstructure of crystals formed from undercooled melts is known from the early work of Nelson and Richardson [21] on aluminum oxide, and was also found in our work in the solidification of deeply undercooled molten alumina under containerless conditions [3]. We found that a highly dendritic, fine-grained microstructure results upon solidification in air or oxygen and that large and dense grains form when the melt is cooled in argon. Liquid oxides dissolve a significant amount of oxygen, (and are also well known to dissolve considerable amounts of water [22]), and the dissolved gas has a large influence on the microstructure of crystallized material.

Additives to YAG compositions were found (small amounts of Nd substituted for Y or a slight excess of alumina) that resulted in easy glass formation and uniform diameter fiber synthesis from the undercooled melts. The additives evidently influence the mechanisms that would otherwise cause imperfections in the fibers. These mechanisms might involve stabilization of a liquid that may otherwise tend to separate into two phases, or buffering of the melt oxygen content. Further investigation of additives is warranted, especially for the mullite compositions. The desired additives would allow pulling of uniform property glass fibers and lead to dense and coarse-rained or single crystalline material upon crystallization of the glass fibers. The additives should be ones that are easily incorporated into the structure of the crystalline material, such as Nd in YAG.

The curved solidus at the silica-rich edge of the mullite phase, shown in the phase diagram determined by Prochazka and Klug suggests a final mechanistic point of interest. They showed that the mullite phase boundary departs 40:60 SiO_2:Al_2O_3 at a temperatures above 1500-1600°C, which is in the range of the mullite recalescence curves shown in Figures 6 and 8. This temperature range exceeds the furnace temperatures employed in the rapid heating experiments that produced fine-grained mullite from the glass fibers. However, it is possible that the mullite fiber crystallization rates were sufficient to heat the fibers to a higher temperature. The rapid heating experiments should be repeated with a mullite-composition glass that is slightly rich in aluminum oxide.

5.4 Synthesis of Longer Glass Fibers

Longer or continuous glass fibers of YAG and mullite compositions are key needs in further R&D to make high quality crystalline fibers for high temperature applications. Continuous processing will permit more precise control of the glass fiber pulling so that fibers with highly reproducible and uniform compositions, diameters and properties will be available. The longer fibers are also needed to improve control in the crystallization experiments, allow crystallization of fibers under tension, for use in high temperature tensile testing and creep measurements, and to allow fiber production in quantities sufficient for applications testing.

The present work has laid the basis for continuous fiber synthesis processes which will be described in the Phase II proposal. Key aspects of the proposed methods are the use of contained melts, with temperature gradients that permit undercooling at the free liquid

surface, while the melt in contact with the container remains at a higher temperature. Opposed fiber drawing methods may also be employed to minimize the motions induced by the fiber pulling force. Measurements of the fiber pulling force will be possible to provide data needed to control the process and design methods to make commercial quantities of the fibers.

5.5 Crystallization of Continuous Glass Fibers

Figure 29 illustrates the concept we have developed to crystallize continuous glass fibers. The top part of the figure shows the apparatus, which consists of a small furnace heated to about 1300K, at which temperature the nucleation and growth of crystals from the glass will spontaneously occur. A feed spool feeds glass fiber to the furnace and a take-up spool receives crystalline fiber formed in the furnace. Temperature gradients occur near the entrance and exit of the furnace as indicated just below the apparatus drawing.

The bottom part of the figure shows how the nucleation of crystals, crystal growth process, and heat release that occurs with crystallization will influence the process. This figure shows the temperature-time history of a section of the fiber as it enters the entrance to the furnace. The shaded region is the TTT curve, i.e., the region of the time-temperature curve in which transformation to crystals will occur. If the fiber did not crystallize, the temperature of the section would increase with the local furnace temperature as it enters the furnace and exhibit the temperature vs time behavior shown by the dashed line. The line enters the shaded region of the TTT curve, where crystallization is initiated and crystalline material is formed at a temperature much above the local furnace temperature as a result of the heat released. Heat flows from the hot crystal to the adjacent glass, causing the glass to follow a new temperature-time curve shown by the solid line in the figure. This now temperature-time curve does not enter the TTT region, so that nucleation of new crystals in the glass is avoided. If the direction of crystal growth can be induced to be on the fiber axis, it becomes possible for a single crystal to grow continuously, yielding a single crystal fiber. Otherwise, the crystal would stop growing at the edge of the fiber, allowing a new crystal to be formed by heterogeneous nucleation at a slower growing surface of the original crystal.

The challenges in controlling continuous crystal growth and methods for their solution will be discussed in our Phase II proposal.

References

1. P.C. Nordine, J.K.R. Weber and J.J. Felten, "Fiber Drawing from Undercooled Molten Materials," US Patent Application no. 08/807,580, Apr., 1997.

2. W.M. Kriven, M.H. Jilavi, D. Zhu, J.K.R. Weber, B. Cho, J.J. Felten and P.C. Nordine, "Synthesis and Microstructure of Mullite Fibers Grown from Deeply Undercooled Melts," Proc. Pask Symposium, 1996, in press.

3. J.K.R. Weber, C.D. Anderson, S. Krishnan and P.C. Nordine, "Solidification Behavior of Undercooled Liquid Aluminum Oxide," J. Am. Ceram. Soc., **78**, 577-82 (1995).

4. J.K.R. Weber, P.C. Nordine, K.C. Goretta, and R.B. Poeppel, "Effects of Oxygen Pressure on the Structure of Y-Ba-Cu-O Materials Formed by Containerless Melting and Solidification," J. Mat. Res. **9**, 1657-60 (1994).

5. S.H. Risbud and J.A. Pask, "Mullite Crystallization from SiO_2-Al_2O_3 Melts," J. Am. Ceram. Soc., 61, 63-67 (1978).

6. S. Aramaki and R. Roy, "Revised Phase Diagram for the System Al_2O_3-SiO_2," J. Am. Ceram. Soc., **45**, 229 (1962).

7. S. Prochazka and F.J. Klug, "Infrared-Transparent Mullite Ceramic," J. Am. Ceram. Soc. **66**, 874 (1983).

8. G.T. Adylov, G.V. Voronov, E.P. Mansurova, L.M. Sigalov and E.M. Urazaeva, "Phase Diagram of Y_2O_3-Al_2O_3," Russ. J. Inorg. Chem., **33**, 1062-63 (1988).

9. J.K.R. Weber, J.J. Felten and P.C. Nordine, "New Method for High Purity Ceramic Synthesis," Rev. Sci. Instrum., **67**, 522-24 (1996).

10. M. Mizuno and H. Saito, "Preparation of Highly Pure Fine Mullite Powder, J. Am. Ceram. Soc., **72**, 377-82 (1989).

11. J.K.R. Weber and P.C. Nordine, "Containerless Liquid-Phase Processing at High Temperatures," Microgravity Science and Technology, VII, 279-282 (1995).

12. J. Coutures and J.P. Coutures, private communication.

13. I.C. Lin, A. Navrotsky, private communication.

14. N.P. Bansal and R.H. Doremus, "Determination of Reaction Kinetic Parameters from Variable Temperature DSC or DTA," J. Thermal Anal., **29**, 115-119 (1984).

15. D.A. Porter and K.E. Easterling, Phase Transformations in Metals and Alloys, pp. 261-381, Chapman & Hall, New York, 1992.

16. N.P. Bansal, R.H. Doremus, A.J. Bruce, and C.T. Moynihan, "Kinetics of Crystallization of ZrF_4-BaF_2-LaF_3 Glass by Differential Scanning Calorimetry," J. Amer. Cer. Soc, **66**, 233-238 (1983).

17. N.P. Bansal and M.J. Hyatt, "Crystallization Kinetics of BaO-Al_2O_3-SiO_2 Glasses," J. Mater. Res., **4**, 1257-1265 (1989).

18. C.A. Angell, "Formation of Glasses from Liquids and Biopolymers," Science, **267**, 1924-35 (1995)

19. S. Aasland and P.F. McMillan, "Density-driven Liquid-liquid Phase Separation in the Al_2O_3-Y_2O_3 System," Nature, **369**, 633 (1994).

20. V.J. Fratello and C.D. Brandle, "Physical Properties of a $Y_3Al_5O_{12}$ Melt," J. Cryst. Growth, **128**, 1006-10 (1993).

21. L.S. Nelson, N.L. Richardson, K. Keil and S.R. Skaggs, "Effects of Oxygen and Argon Atmospheres on Pendant Drops of Aluminum Oxide Melted with Carbon Dioxide Laser Radiation," High Temp. Sci., **5**, 138-154 (1973).

22. J.J. Diamond and A.L. Dragoo, "Studies of Molten Alumina in the Arc-Image Furnace," Rev. Int. Hautes Temper. et Refract., **3**, 273-79 (1966).

Table I. Binary alumina-silica and alumina-yttria compositions which were investigated.

Chemical Composition		Comments
Mol % Al_2O_3	Mol % SiO_2	Processed in a pure Ar, O_2 or air
50	50	Pulled in O_2
54	46	Pulled in O_2
59	41	Pulled in Ar
60	40	Pulled in air
60	40	Pulled in O_2
60	40	Pulled in O_2, Kyoritsu mullite
61	39	Pulled in Ar
62	38	Pulled in Ar
64	36	Pulled in Ar
Mol % Al_2O_3	Mol % Y_2O_3	Processed in a pure Ar atmosphere
62.5	37.5	Mixed oxide powders
62.5	37.5	Crushed single crystal
63.5	36.5	Mixed oxide powders
65.0	35.0	Mixed oxide powders
76.0	24.0	Mixed oxide powders
62.5	36.5	1 mol % Nd_2O_3 substituted for Y_2O_3
62.5	36.5	1 mol % Er_2O_3 substituted for Y_2O_3
63.5	35.5	1 mol % Er_2O_3 substituted for Y_2O_3

Table II. Tensile fracture strength for 36.5 Y_2O_3, 62.5 Al_2O_3, 1.0 Nd_2O_3 glass fibers

No.	Condition	Fracture Strength, GPa
1	Preliminary	2.47
2	Preliminary	2.34
3	Selected fiber	5.43
4	Selected fiber	4.67
5	Selected fiber	4.99

Table III. Kinetic data on the crystallization behavior of glassy mullite and glassy YAG obtained from non-isothermal DTA studies.

	Glassy Mullite		Glassy YAG	
α, °C/min	Tp, °C	n	Tp, °C	n
2.5	974.1	3.54	924.1	4.88
5	984.9	4.48	935.3	6.19
10	992.9	5.72	953.7	8.04
20	1,000.9	4.52	964.6	6.38
30	1,006.9	3.79	967.6	5.33
40	1,014.1	2.70	976.5	3.81
E, KJ/mole	952.87		637.06	
ν, s^{-1}	1.46E+39		8.27E+26	

Table IV. Selected results from TTT diagrams for glassy mullite and glassy YAG.

Temperature, °C	Time for 100% crystallization of glassy mullite, sec	Time for 100% crystallization of glassy YAG, sec
1000	17	3
1050	0.541	0.326
1100	0.024	0.040
1200	8E-5	9E-4

Table V. Heating conditions for fiber crystallization.

Material	Heating Rate, °C/min	Maximum Temperature, °C
Mullite	5	1,100
"	10	985
"	10	900
"	10	900
YAG	5	1200
"	5	1100
"	5	1000
"	10	900
"	10	900

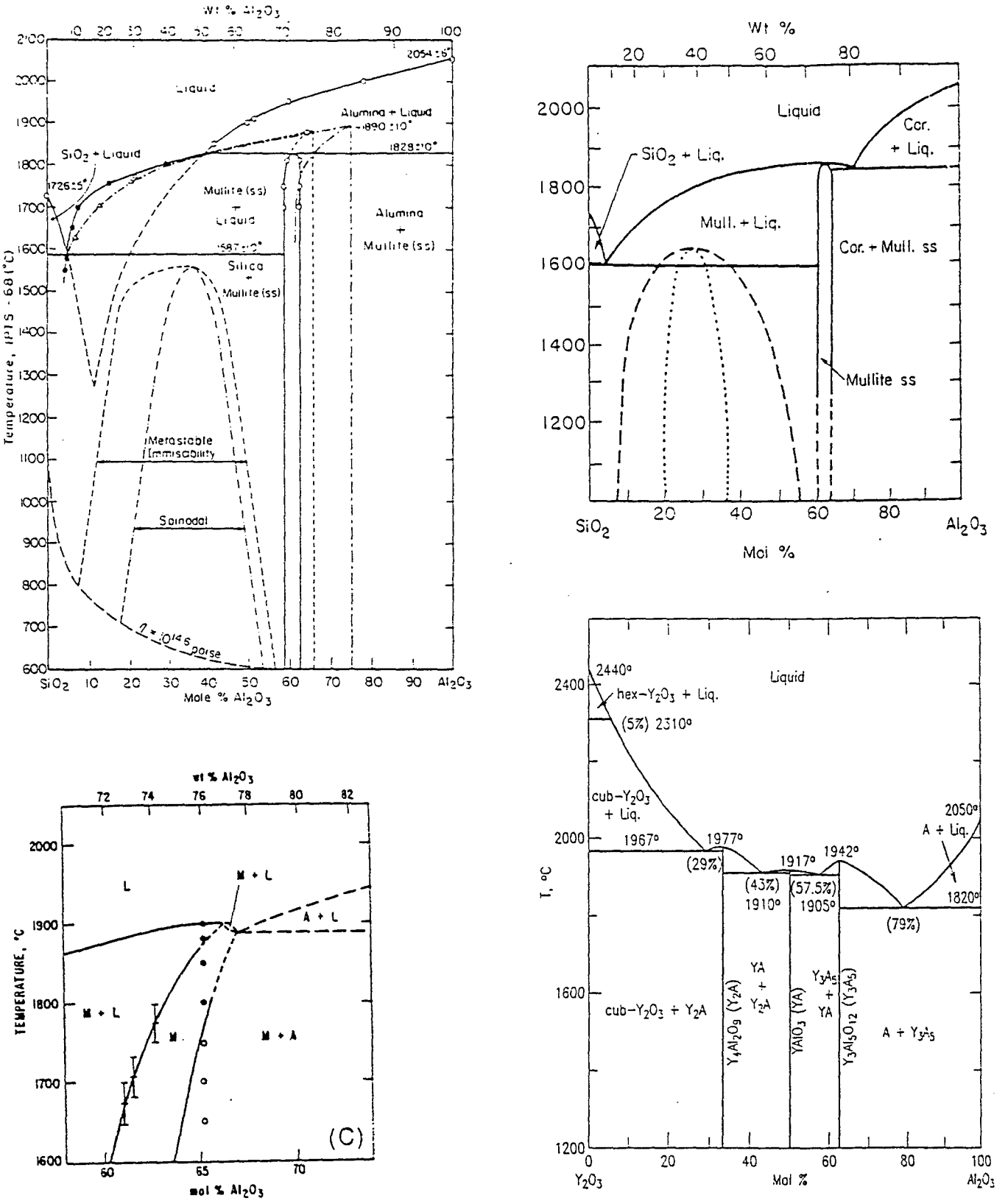

Figure 1. Binary phase diagrams. Top left and right, bottom left: alumina-silica system. Bottom right: alumina-yttria systems.

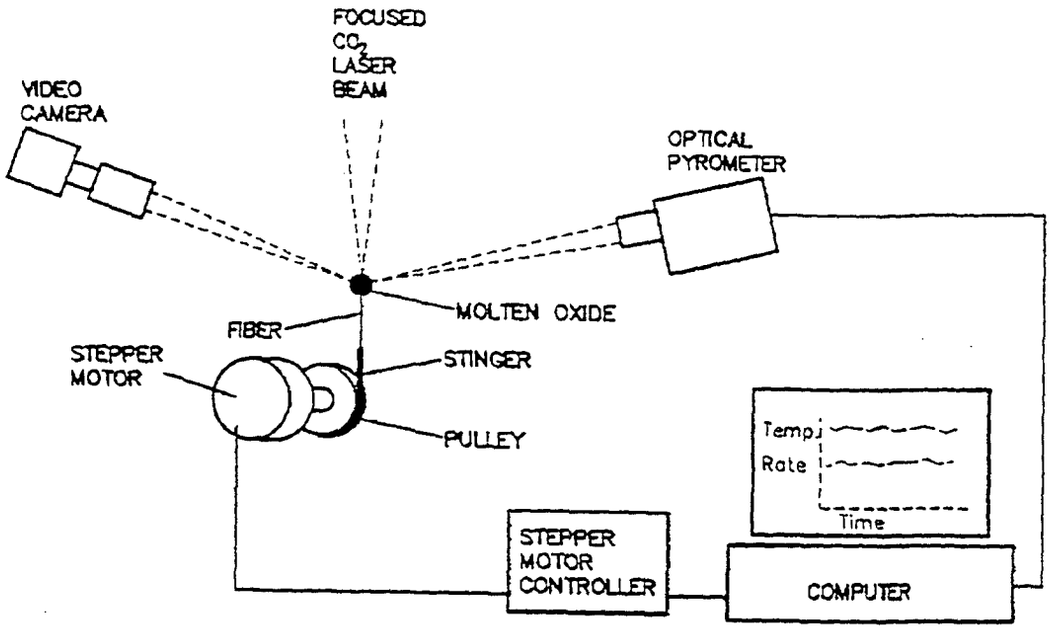

Figure 2. Schematic illustration of the apparatus used for fiber pulling from undercooled melts.

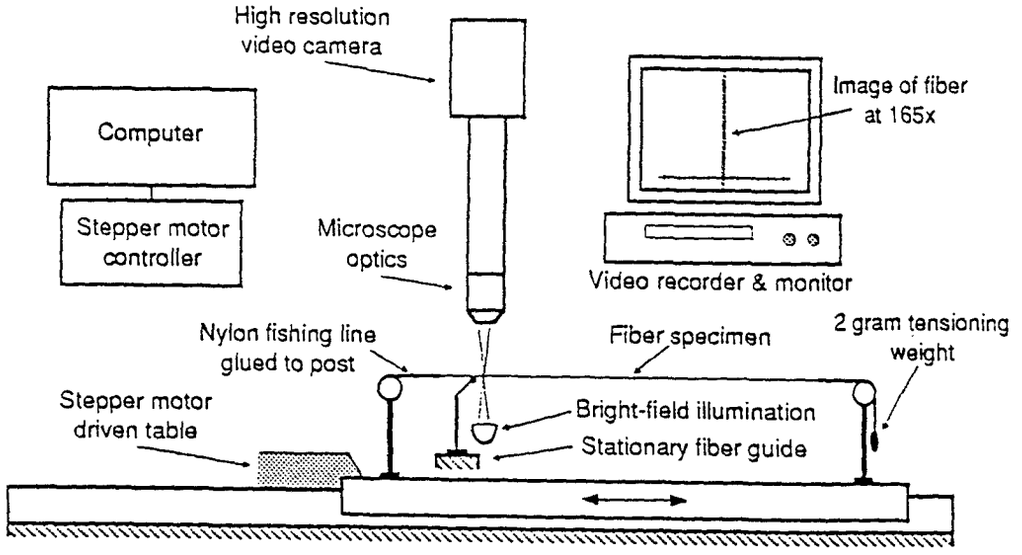

Figure 3. Schematic illustration of the video microscope fiber inspection assembly.

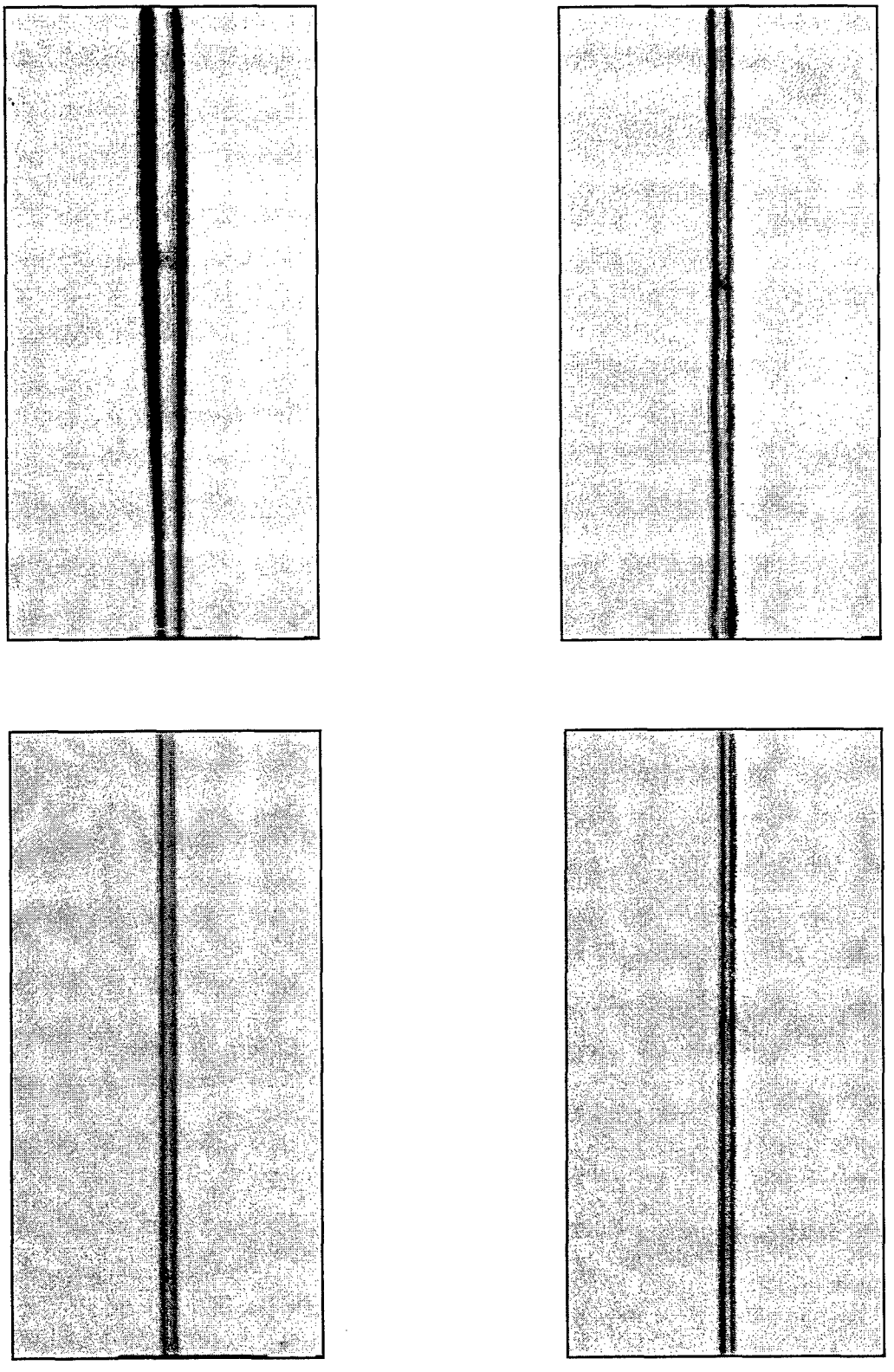

Figure 4. Video microscope pictures of fibers. Left: mullite-, right: YAG-composition. Top: fibers with defects. Bottom: smooth, uniform diameter sections.

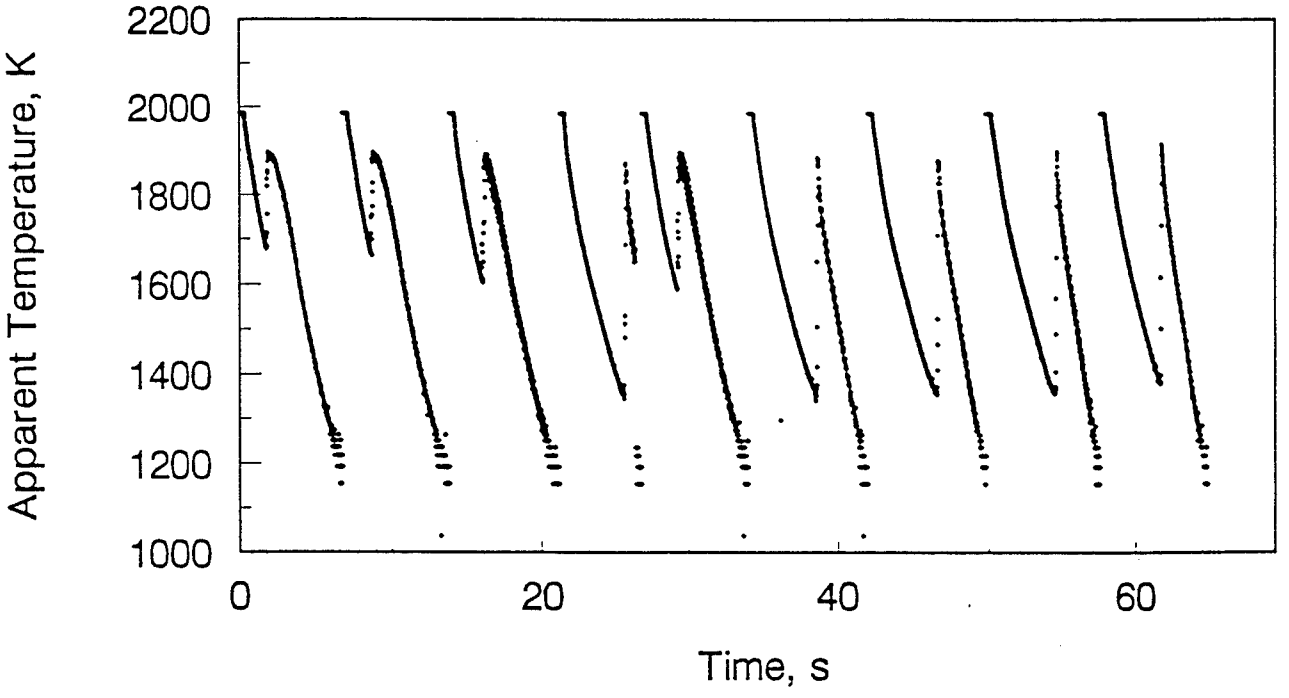

Figure 5. Temperature *vs* time plots for YAG-composition material processed under containerless conditions.

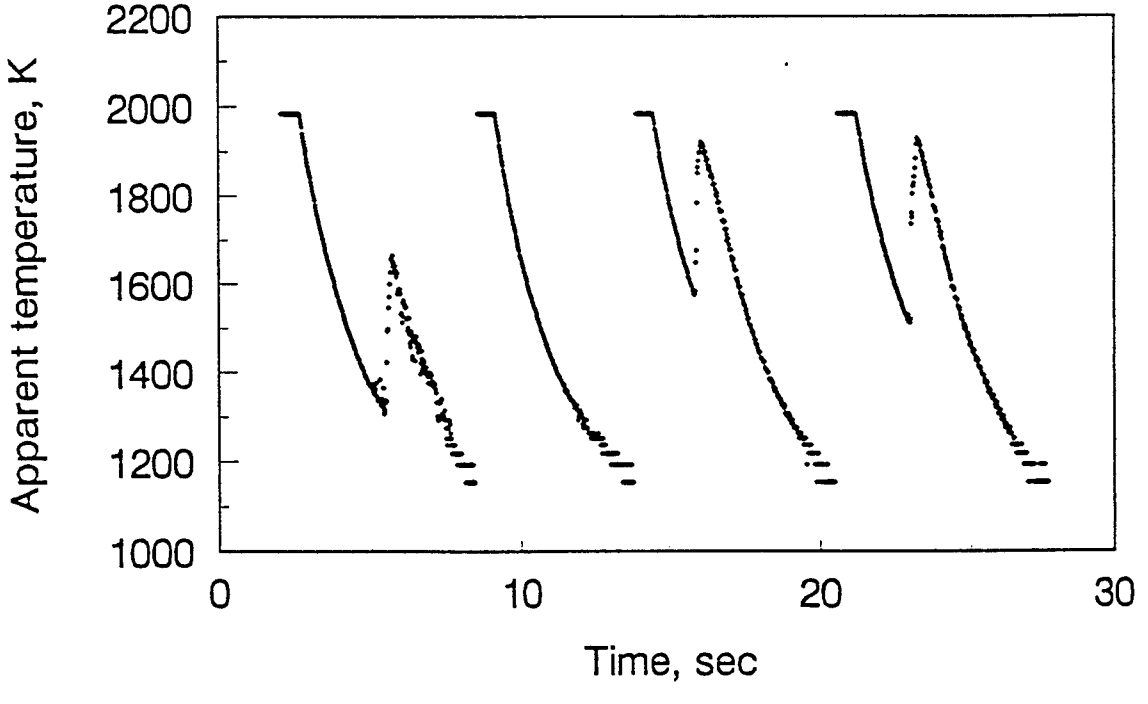

Figure 6. Temperature *vs* time plots for mullite-composition material processed under containerless conditions.

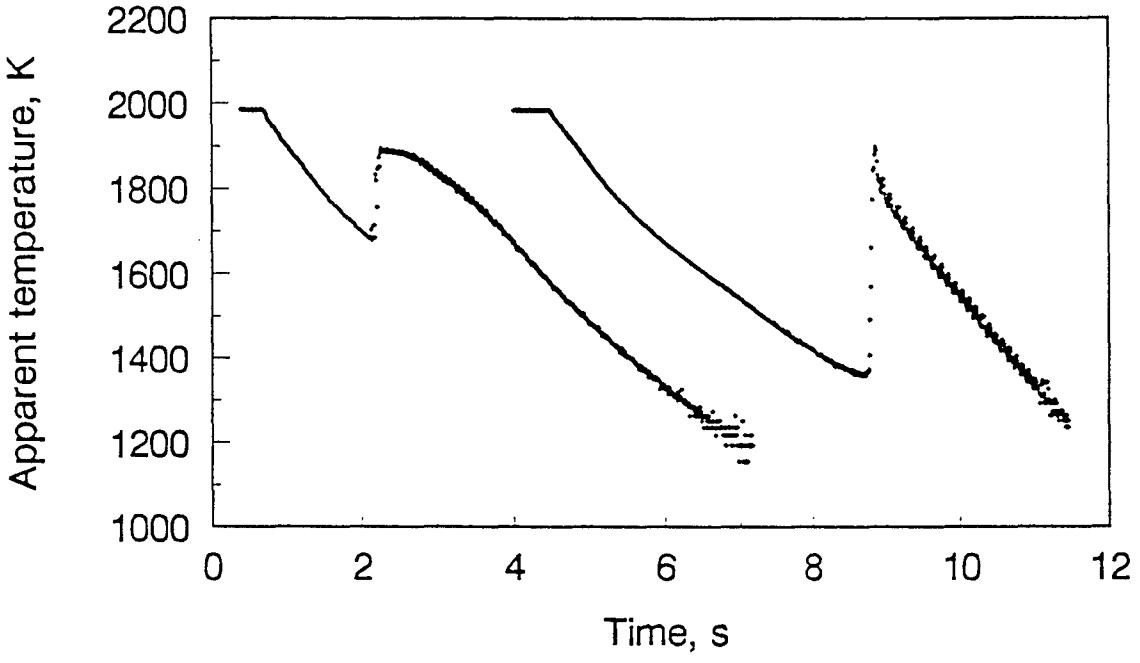

Figure 7. First and last cooling curve from Figure 5 for YAG-composition melts, and the cooling curve for the 24 mol % Y_2O_3 + 76 mol % Al_2O_3 material.

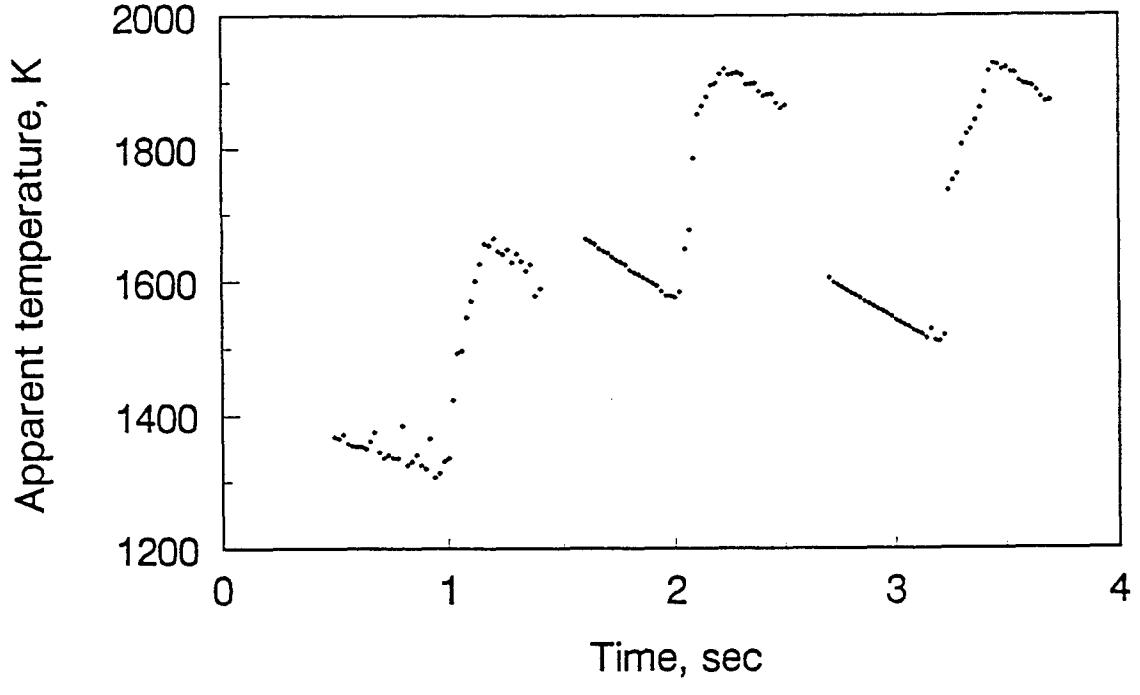

Figure 8. Cooling curves for mullite compositions from Figure 6 for which recalescence occurred, shown with an expanded time scale.

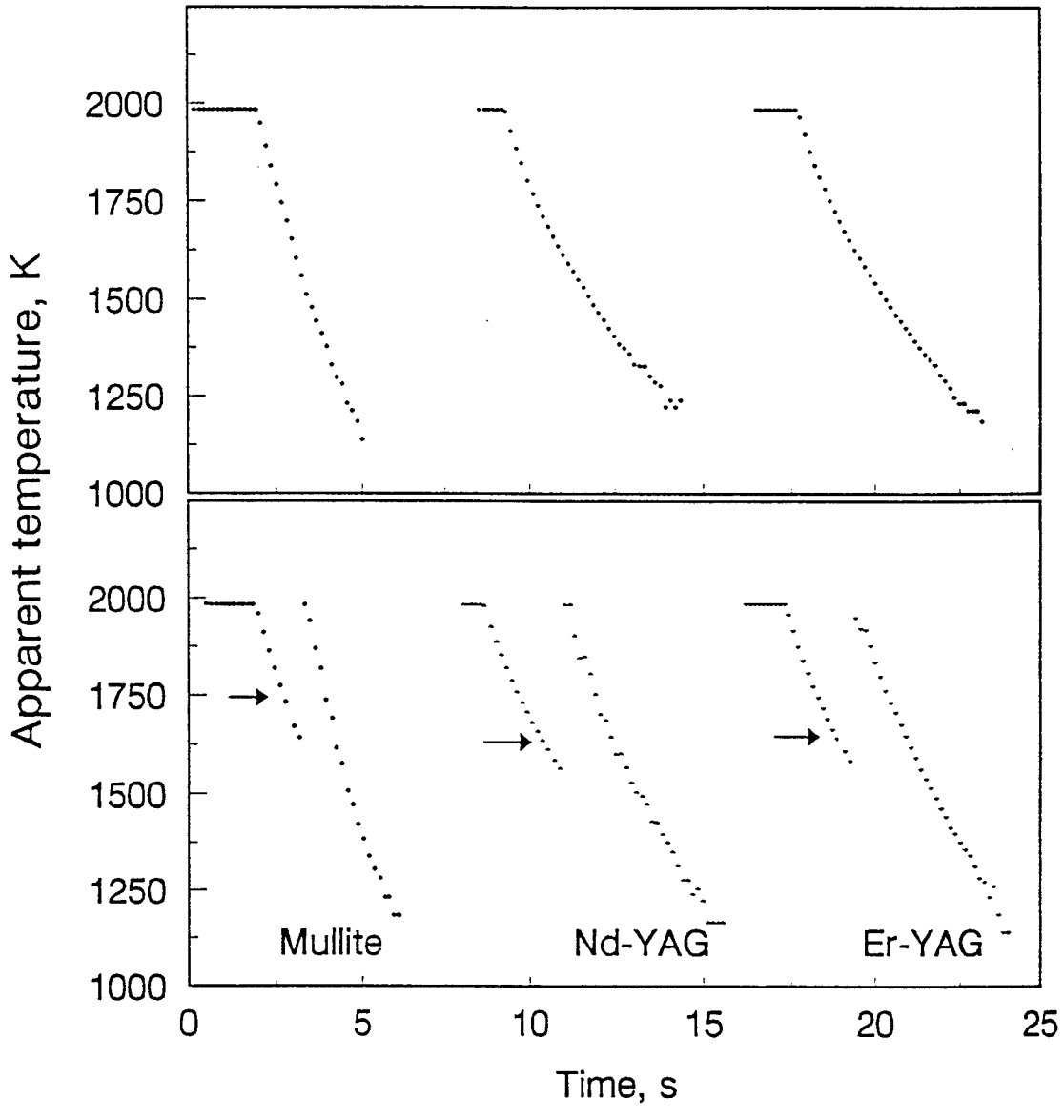

Figure 9. Cooling curves observed in preprocessing and fiber synthesis experiments. The top part shows cooling curves resulting in bulk glass formation for (i) a mullite-composition melt, (ii) a YAG-composition melts with 1 mol % Nd substituted for Y, and (iii) a YAG-composition melt with 1 mol % Er substituted for Y and an excess of 1 mol % Al_2O_3. The bottom part shows the cooling curves obtained for the same materials during fiber pulling experiments. The arrows show the temperature at which stinging and fiber pulling were initiated.

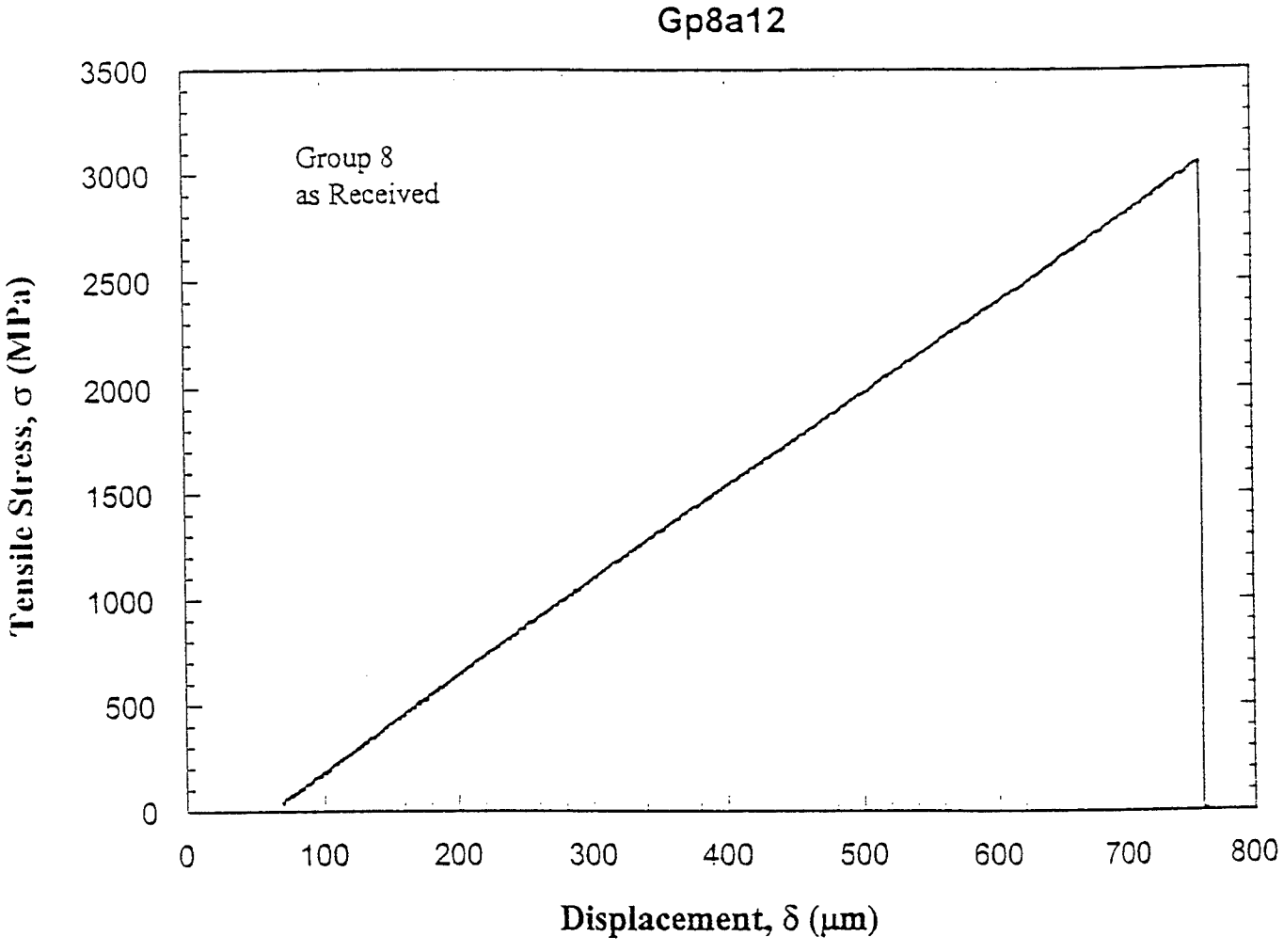

Figure 10. Typical stress *vs* strain plot for a mullite-composition glass fiber.

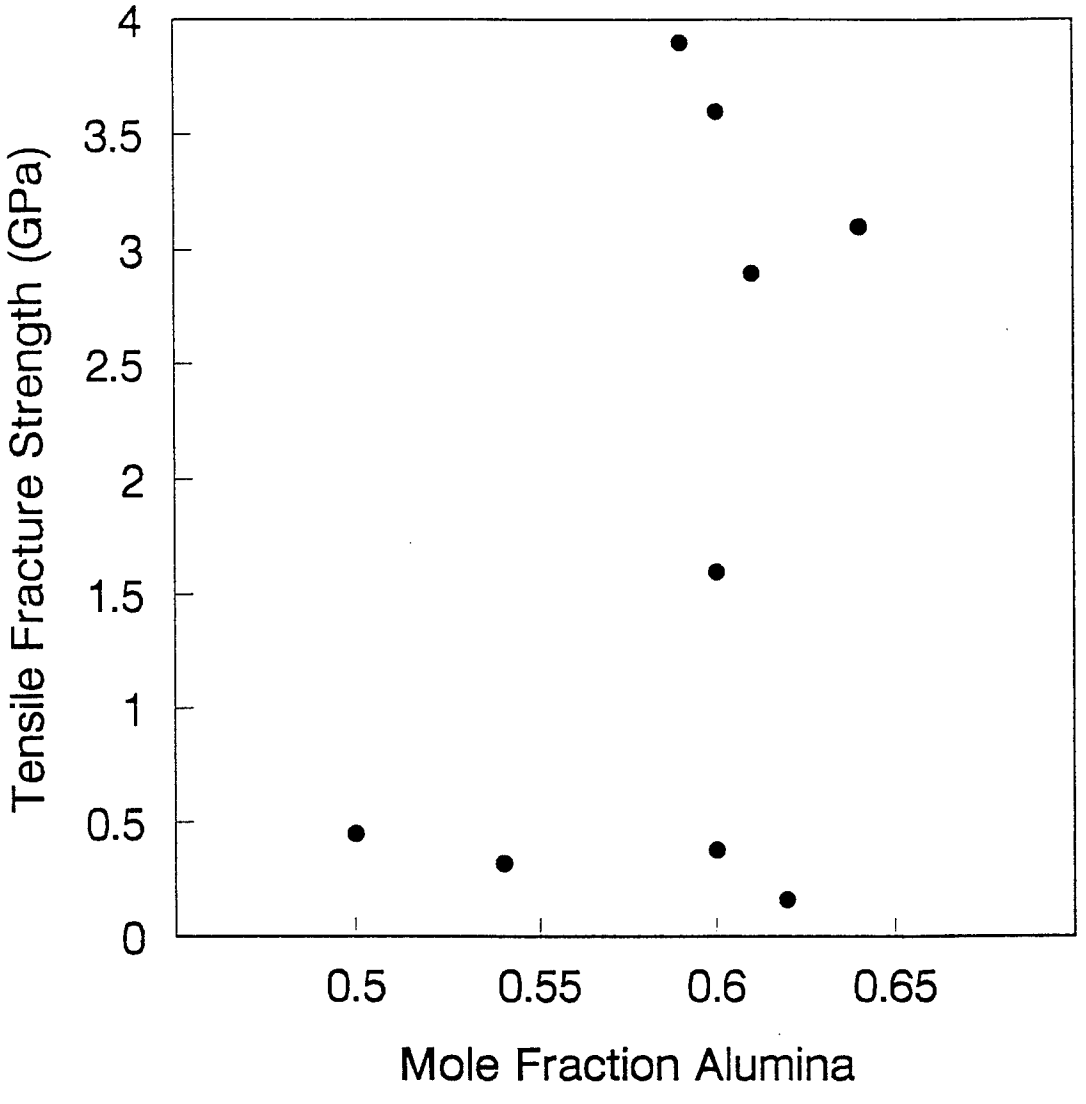

Figure 11. Tensile strengths of binary alumina-silica glass fibers with alumina concentrations from 50-65 mol % alumina shown as a function of composition.

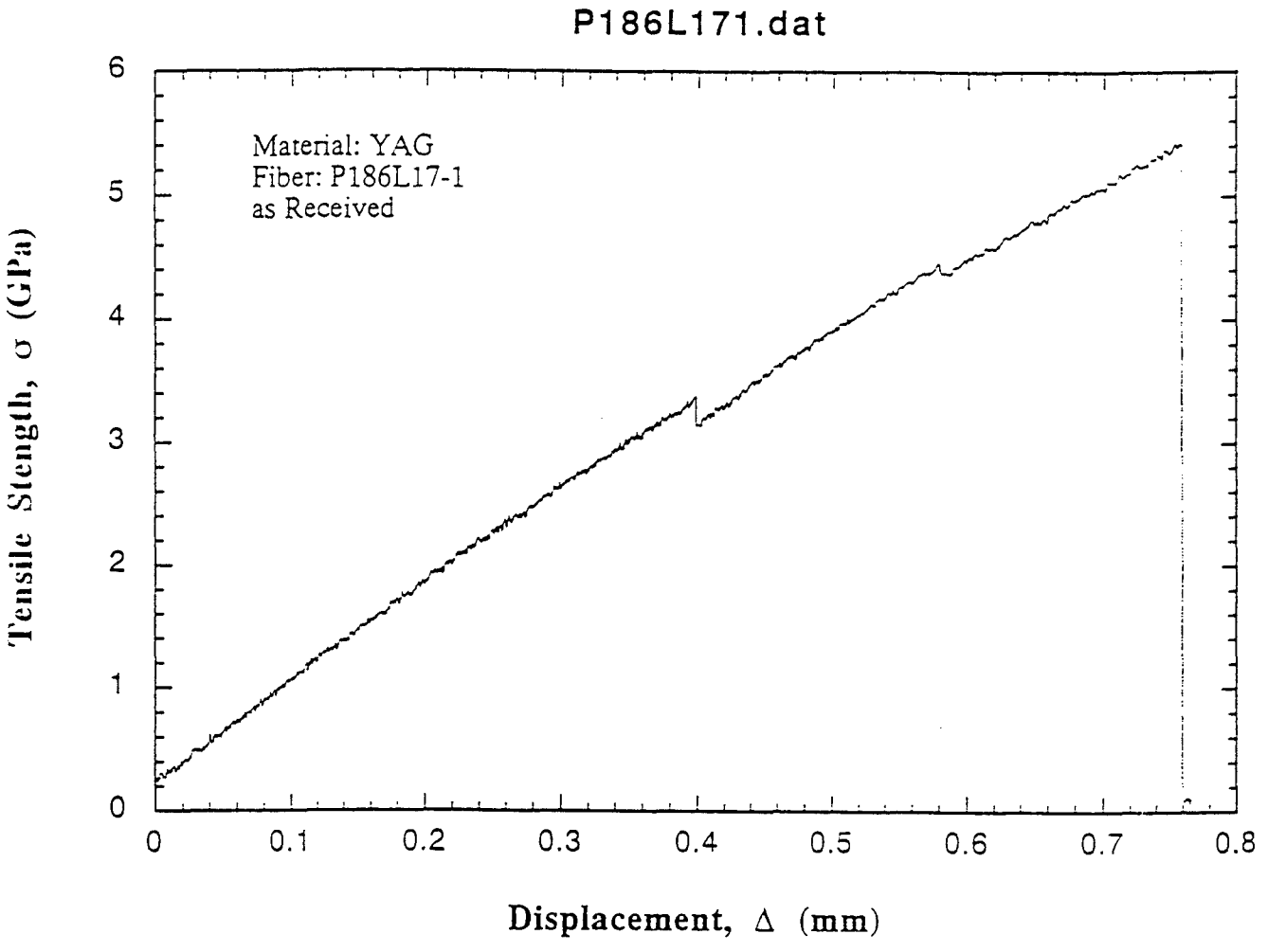

Figure 12. Typical stress *vs* strain plot for a YAG-composition glass fiber with 1 mol % Nd substituted for Y.

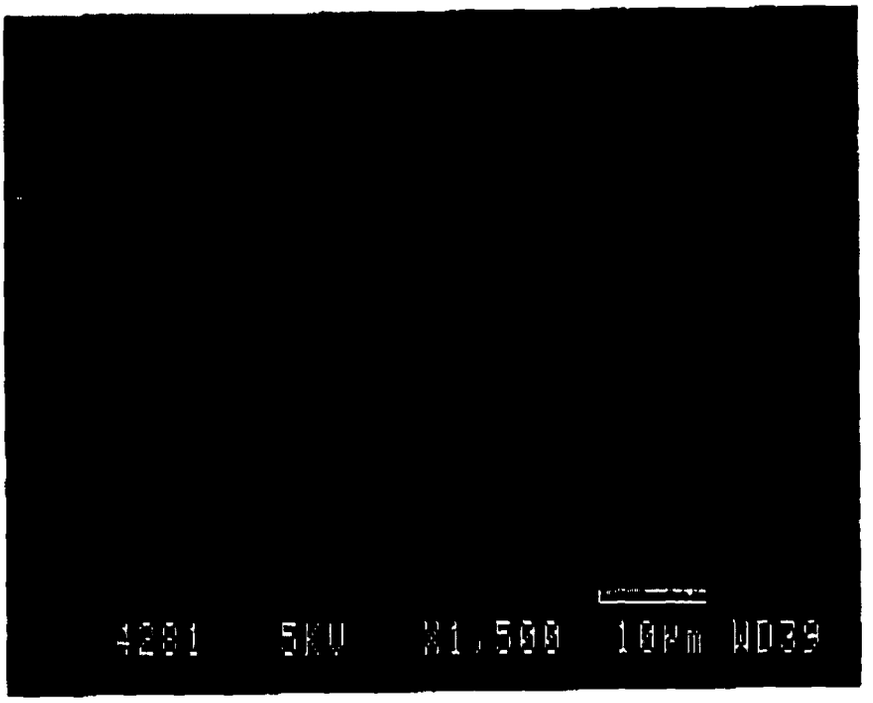

Figure 13. Scanning electron micrograph showing a longitudinal view of a YAG-composition glass fiber.

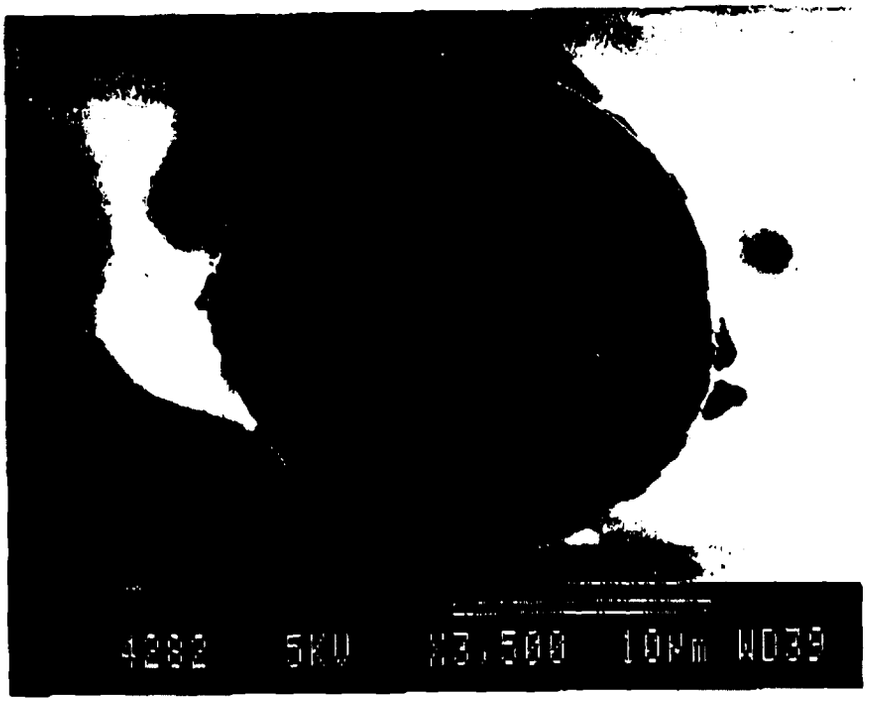

Figure 14. Scanning electron micrograph showing a transverse fracture section of a YAG-composition glass fiber.

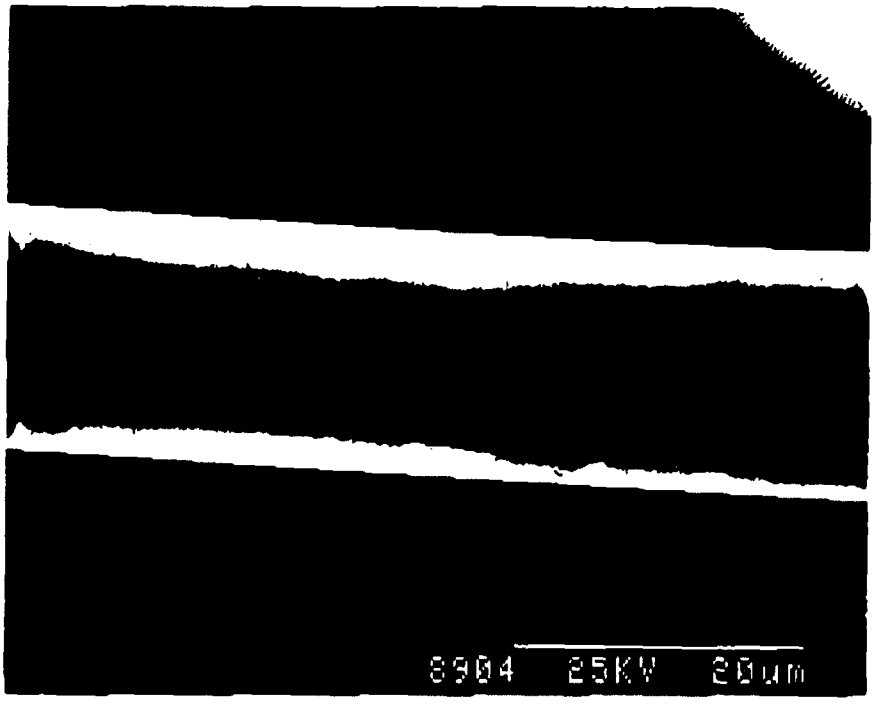

Figure 15. Scanning electron micrograph showing a longitudinal view of a YAG-composition glass fiber made from material with 1 mol% neodymium substituted for yttrium.

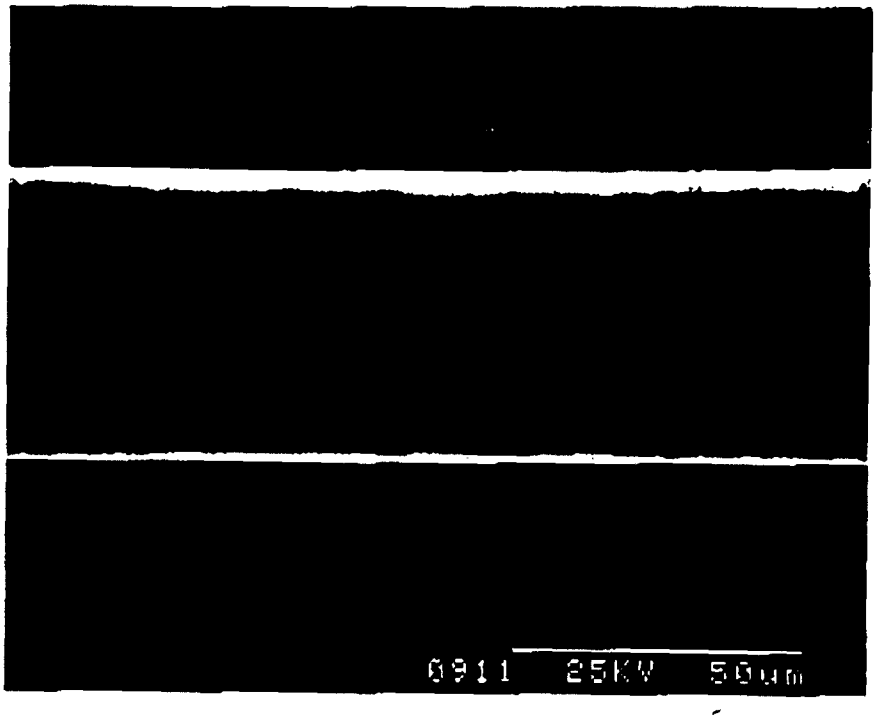

Figure 16. Scanning electron micrograph showing a longitudinal view of a mullite composition glass fiber.

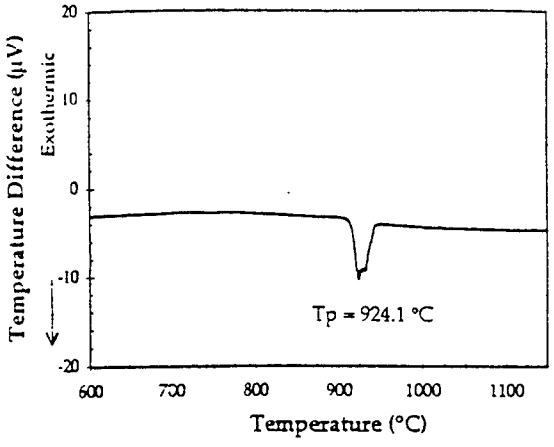

DTA crystallization curve for glassy YAG powder in Ar gas flowing at 75 cc/min using a 2.5 °C/min heat up rate. (8/5/97; 30.08 mg YAG; 24.5 mg Al_2O_3 ref.)

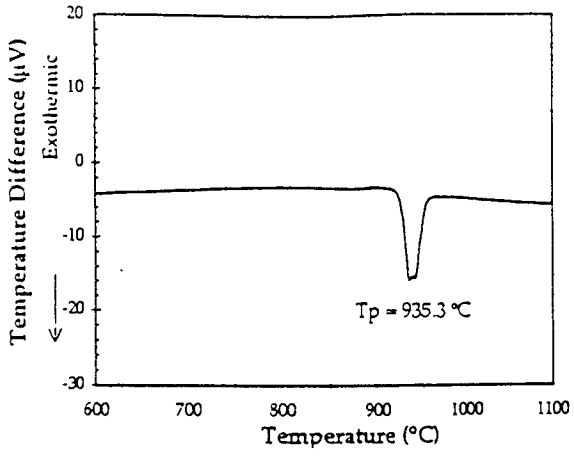

DTA crystallization curve for glassy YAG powder in Ar gas flowing at 75 cc/min using a 5.0 °C/min heat up rate. (8/5/97; 30.20 mg YAG; 24.50 mg Al_2O_3 ref.)

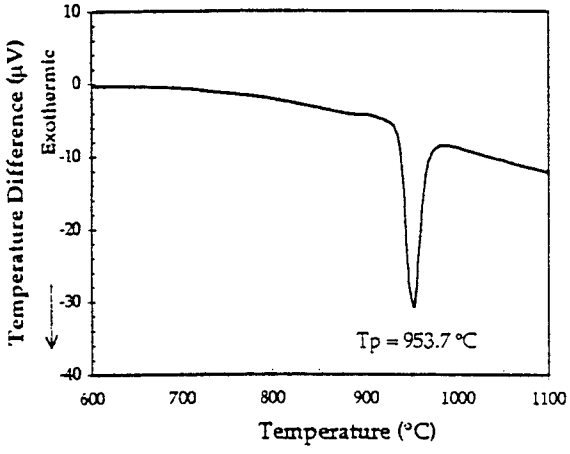

DTA crystallization curve for glassy YAG powder in Ar gas flowing at 75 cc/min using a 10.0 °C/min heat up rate. (8/6/97; 31.00 mg YAG; 24.50 mg Al_2O_3 ref.)

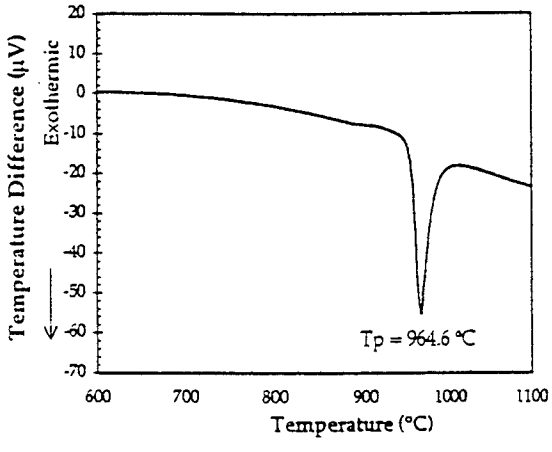

DTA crystallization curve for glassy YAG powder in Ar gas flowing at 75 cc/min using a 20 °C/min heat up rate. (8/6/97; 30.10 mg YAG; 24.50 mg Al_2O_3 ref.)

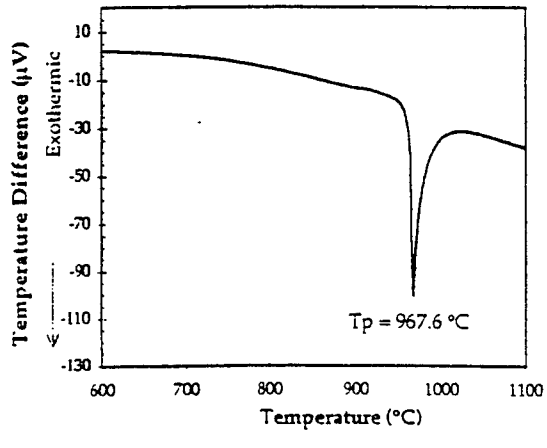

DTA crystallization curve for glassy YAG powder in Ar gas flowing at 75 cc/min using a 30.0 °C/min heat up rate. (8/6/97; 31.30 mg YAG; 24.50 mg Al_2O_3 ref.)

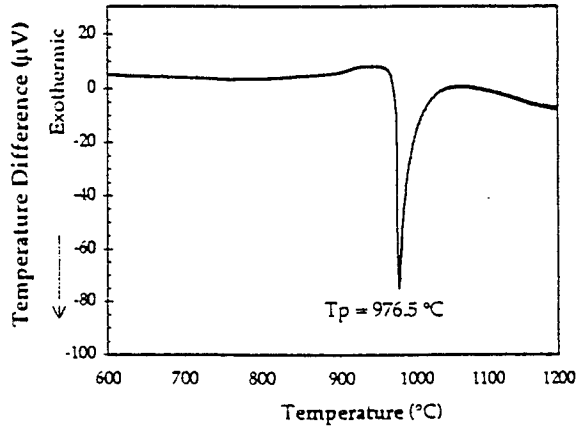

DTA crystallization curve for glassy YAG powder in Ar gas flowing at 75 cc/min using a 40.0 °C/min heat up rate. (8/4/97; 30.00 mg YAG; 24.50 mg Al_2O_3 ref.)

Figure 17. Results of the DTA measurements for glassy YAG for heating rates from 2.5-40°C/min.

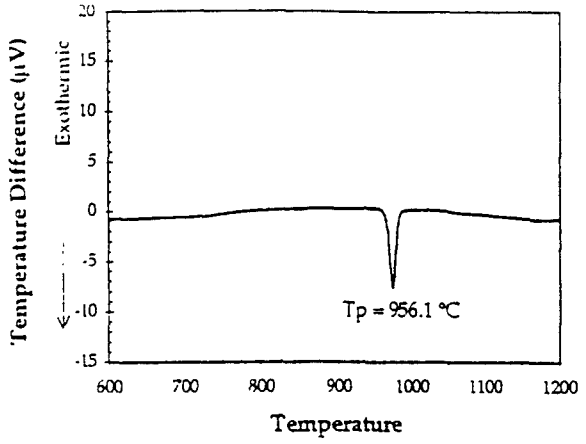

DTA crystallization curve for glassy mullite powder in Ar gas flowing at 75 cc/min using a 2.5 °C/min heat up rate. (6/24/97; 28.90 mg mullite; 36.20 mg Al_2O_3 ref.)

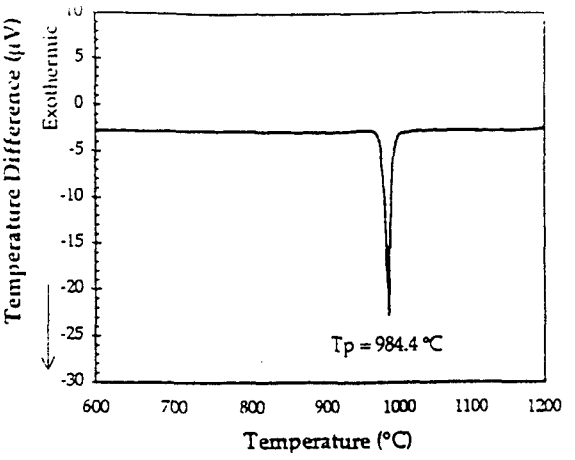

DTA crystallization curve for glassy mullite powder in Ar gas flowing at 75 cc/min using a 5.0 °C/min heat up rate. (6/25/97; 31.50 mg mullite; 36.20 mg Al_2O_3 ref.)

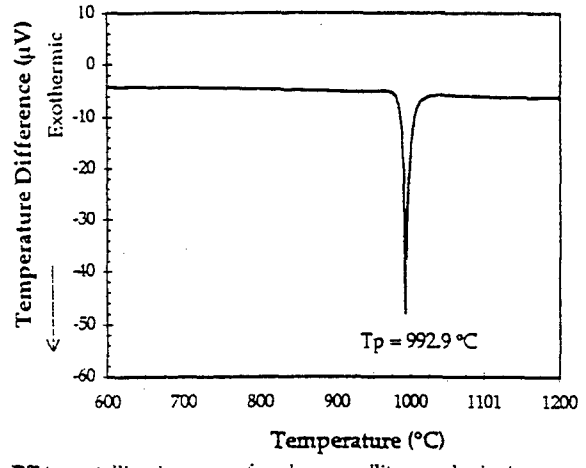

DTA crystallization curve for glassy mullite powder in Ar gas flowing at 75 cc/min using a 10.0 °C/min heat up rate. (6/25/97; 30.90 mg mullite; 36.20 mg Al_2O_3 ref.)

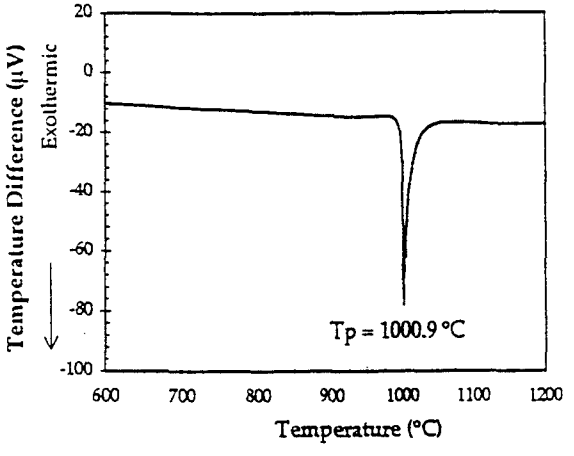

DTA crystallization curve for glassy mullite powder in Ar gas flowing at 75 cc/min using a 20.0 °C/min heat up rate. (6/25/97; 30.50 mg mullite; 36.20 mg Al_2O_3 ref.)

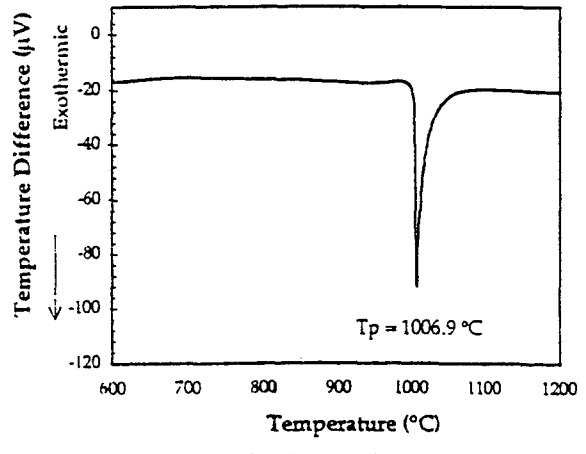

DTA crystallization curve for glassy mullite powder in Ar gas flowing at 75 cc/min using a 30.0 °C/min heat up rate. (6/24/97; 30.30 mg mullite; 36.20 mg Al_2O_3 ref.)

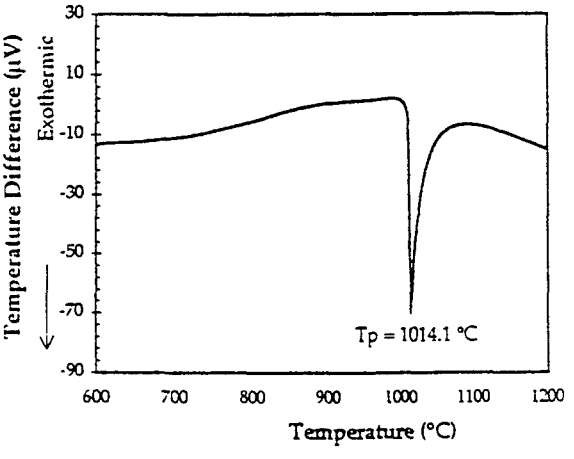

DTA crystallization curve for glassy mullite powder in Ar gas flowing at 75 cc/min using a 40.0 °C/min heat up rate. (6/24/97; 29.70 mg mullite; 36.20 mg Al_2O_3 ref.)

Figure 18. Results of the DTA measurements for glassy mullite for heating rates from 2.5-40°C/min.

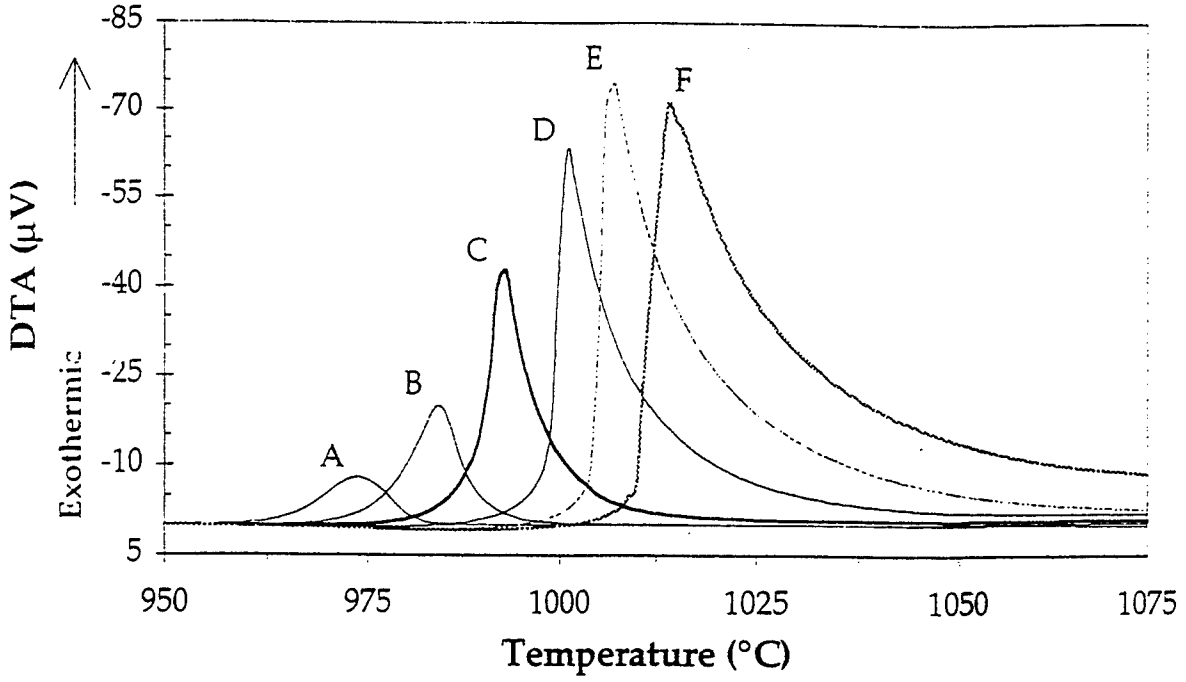

DTA Crystallization curves for glassy mullite at different heating rates normalized to a common baseline. (A = 2.5 °C/ min, B = 5.0 °C/ min, C = 10.0 °C/ min, D = 20.0 °C/ min, E = 30.0 °C/ min and F = 40°C/ min).

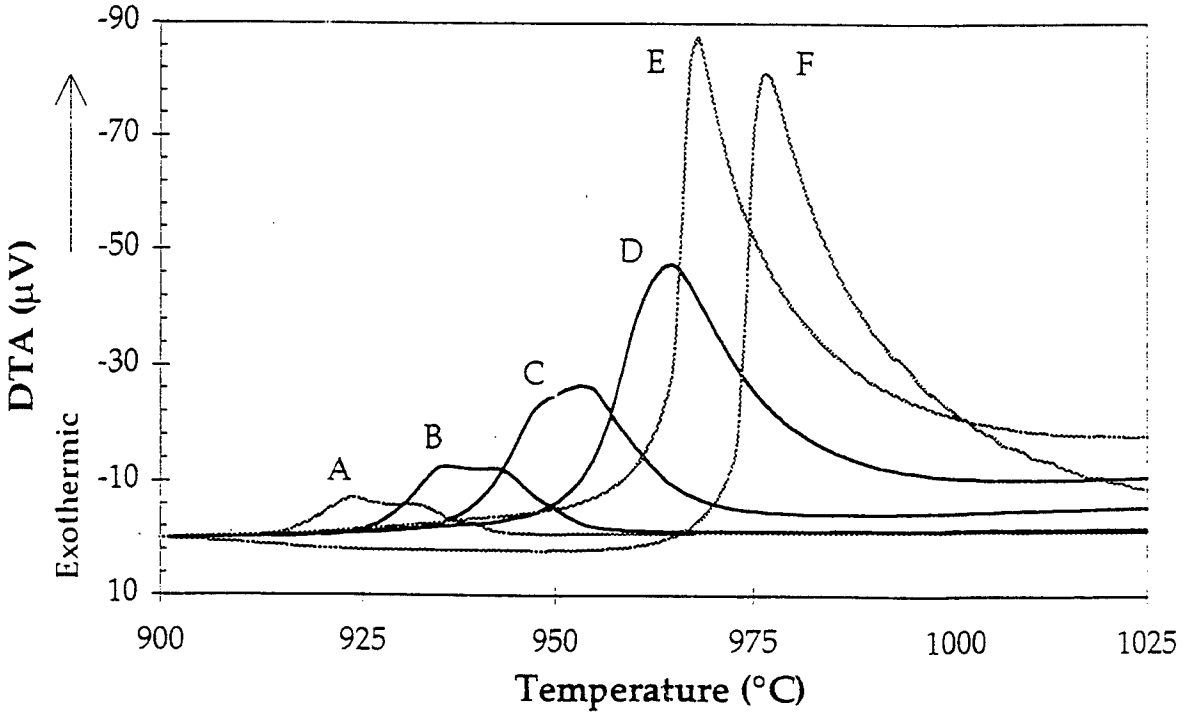

Figure 19. Composite plots showing the DTA results for glassy mullite (top) and glassy YAG (bottom) after normalizing the measurements to a common baseline temperature difference.

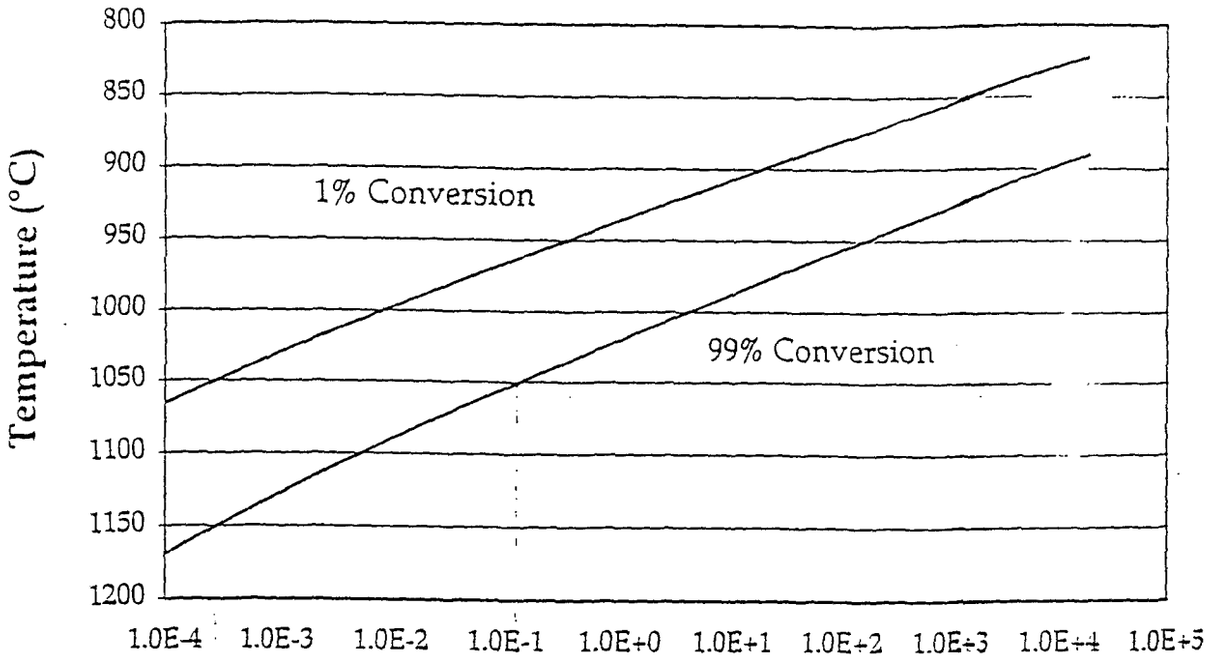

Fig. A

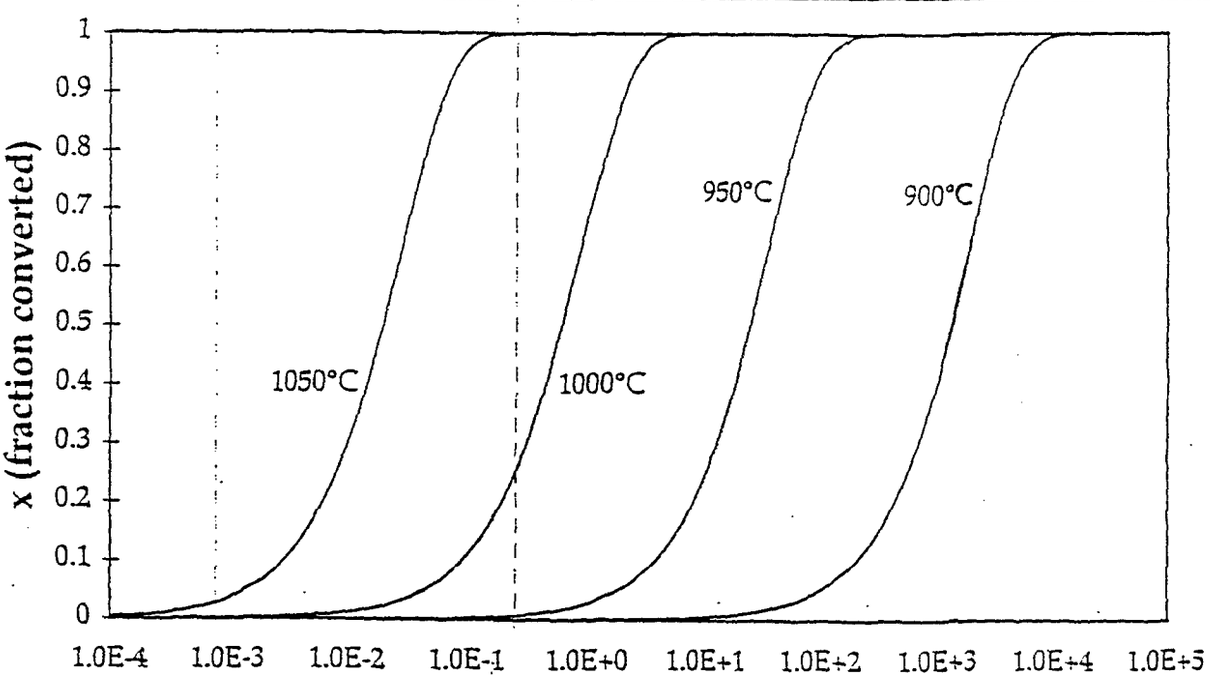

Fig. B

Figure 20. A. (top) Time, temperature, transformation curves for crystallization of glassy mullite (assuming crystal growth in one direction, e.g., along the fiber axis). B. (bottom) The percentage of glassy mullite crystallization as a function of time for various temperatures.

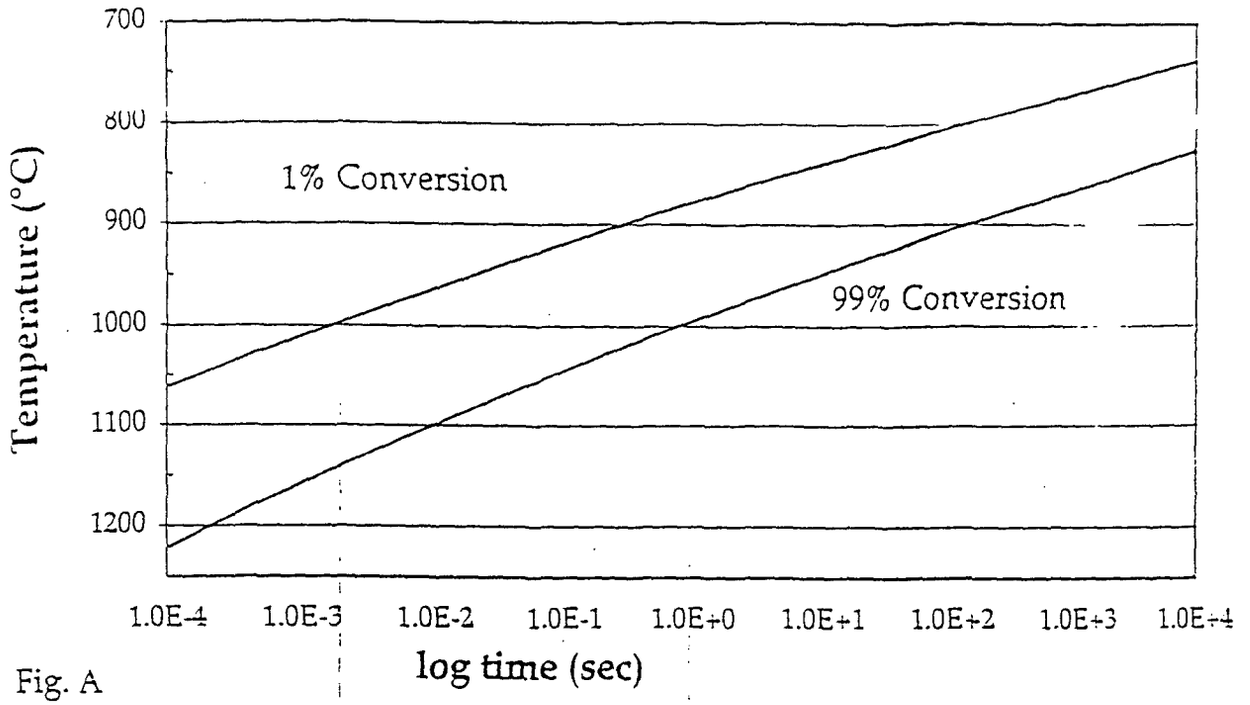

Fig. A

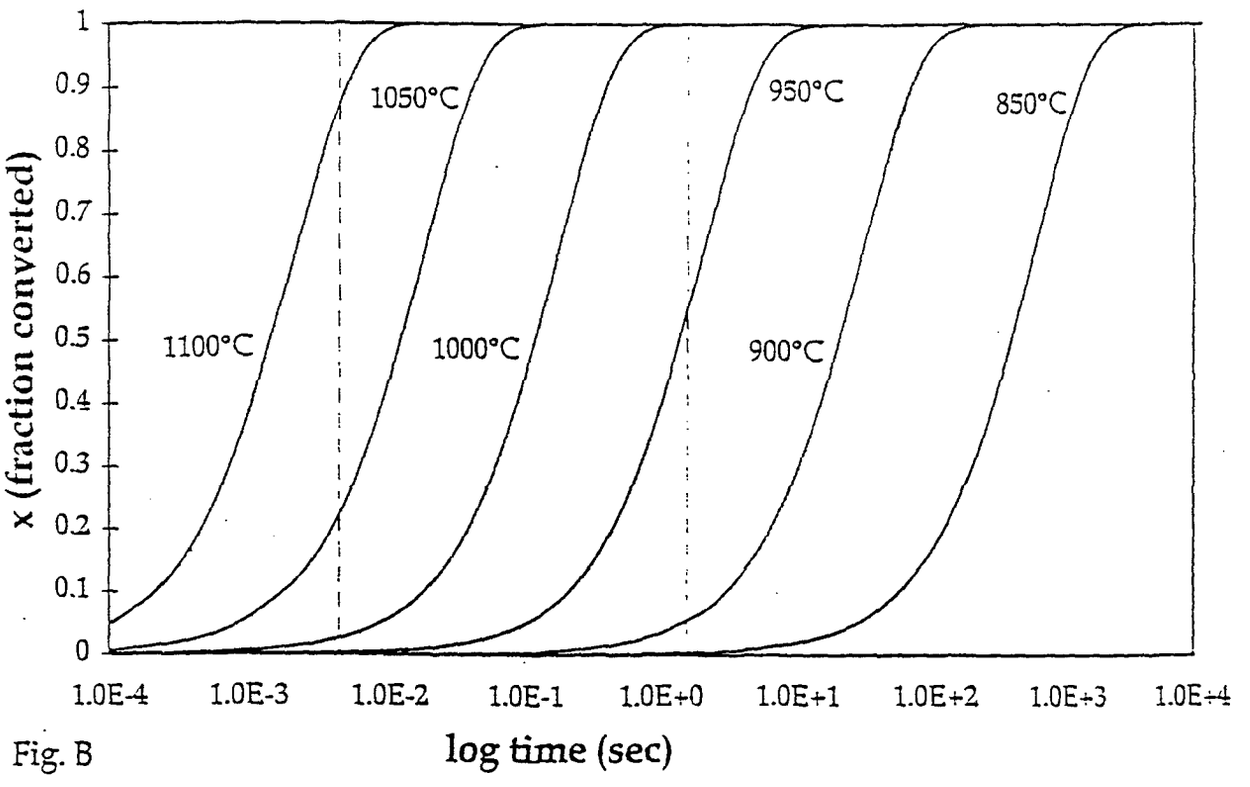

Fig. B

Figure 21. A. (top) Time, temperature, transformation curves for crystallization of glassy YAG (assuming crystal growth in one direction, e.g., along the fiber axis). B. (bottom) The percentage of glassy YAG crystallization as a function of time for various temperatures.

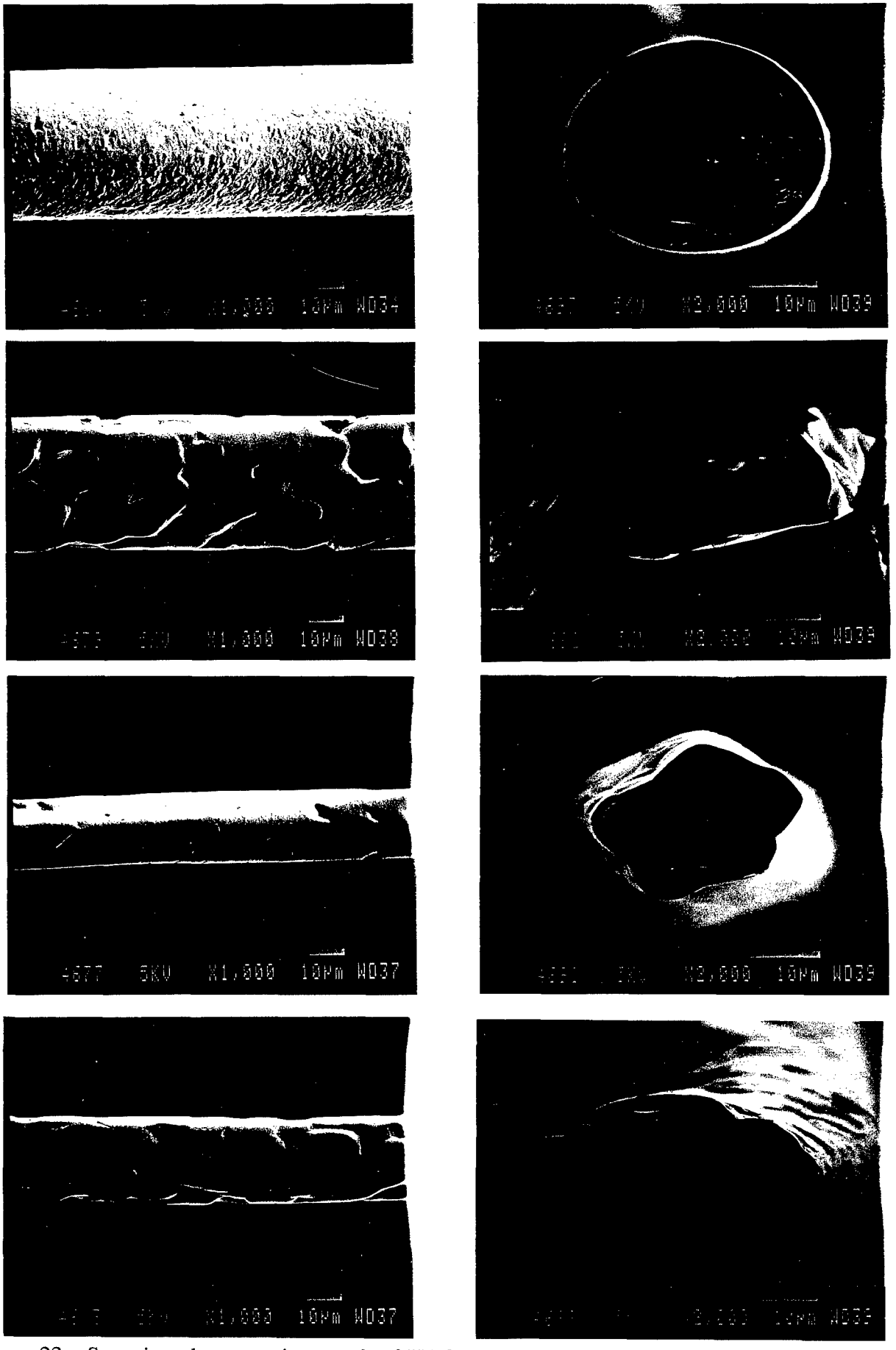

Figure 22. Scanning electron micrograph of YAG-composition fibers crystallized at 1100°C (to 1200°C, 1300°C, and 1400°C (bottom). Left; longitudinal views, right: sections views. Proce time 5 seconds.

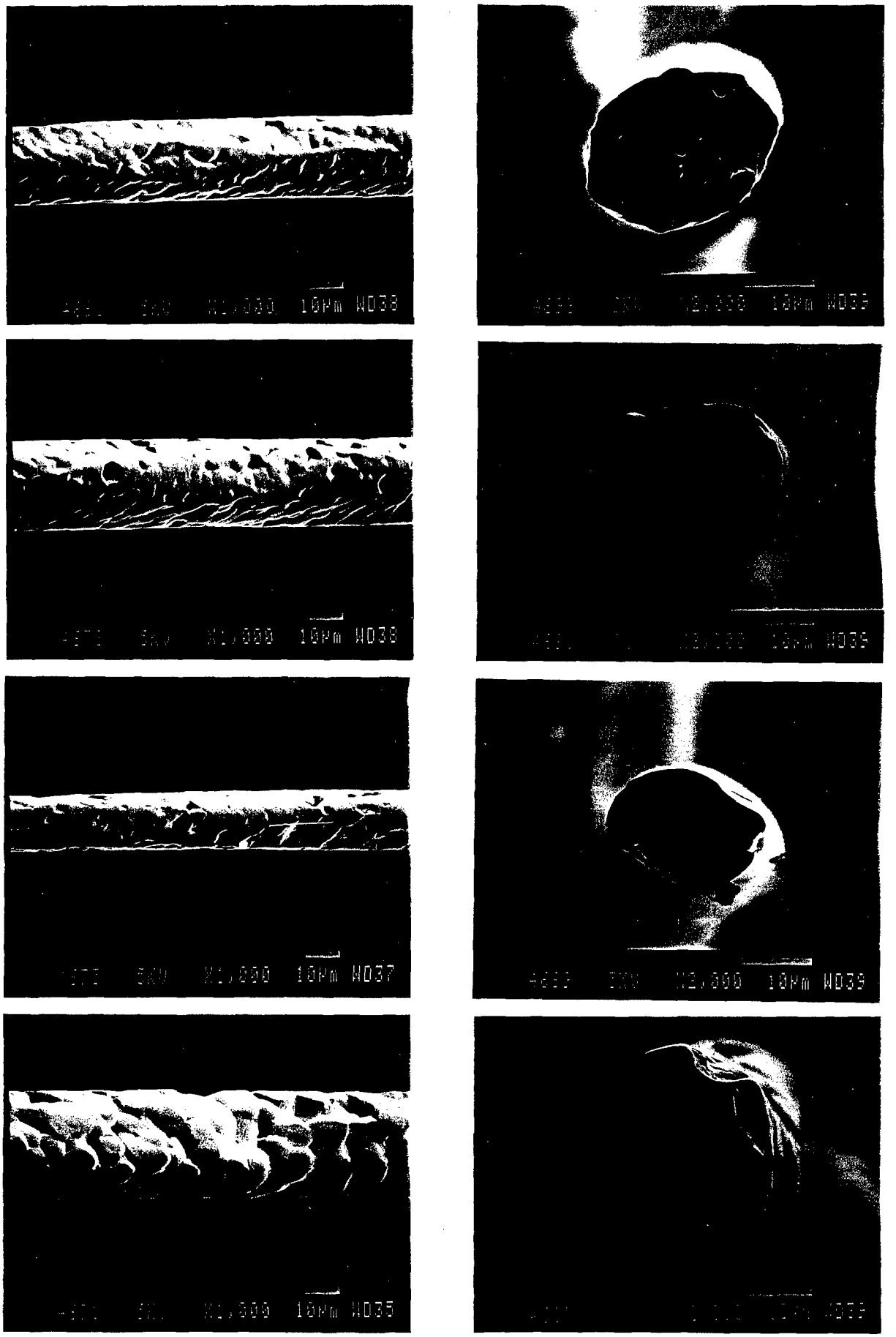

Figure 23. Scanning electron micrograph of YAG-composition fibers crystallized at 1100°C (to 1200°C, 1300°C, and 1400°C (bottom). Left; longitudinal views, right: sections views. Proces time: 15 sec at 1100°C, 30 sec at higher temperatures.

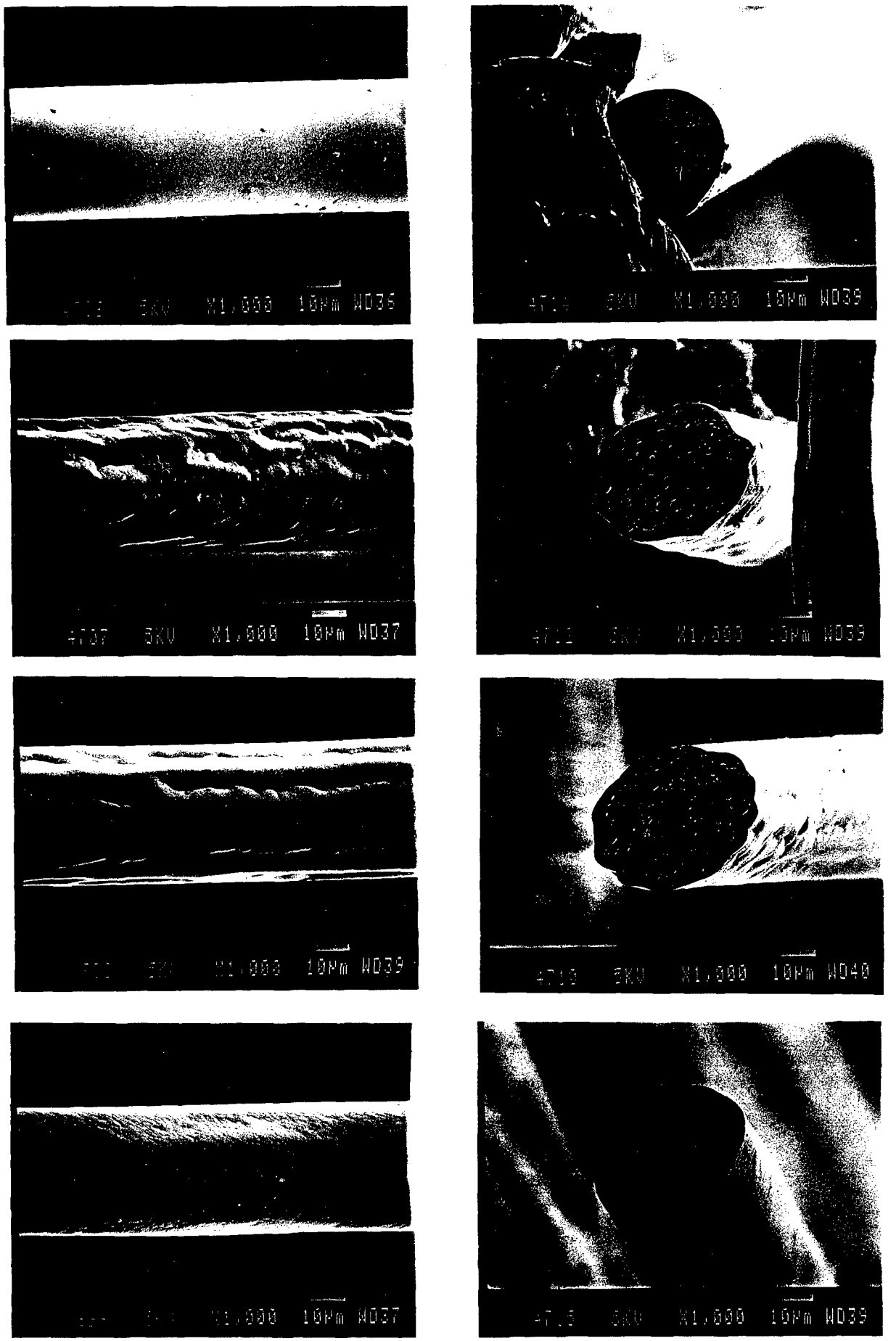

Figure 24. Scanning electron micrograph of mullite-composition fibers crystallized at 1100°C (top) 1200°C, 1300°C, and 1400°C (bottom). Left; longitudinal views, right: sections views. Process time 5 seconds.

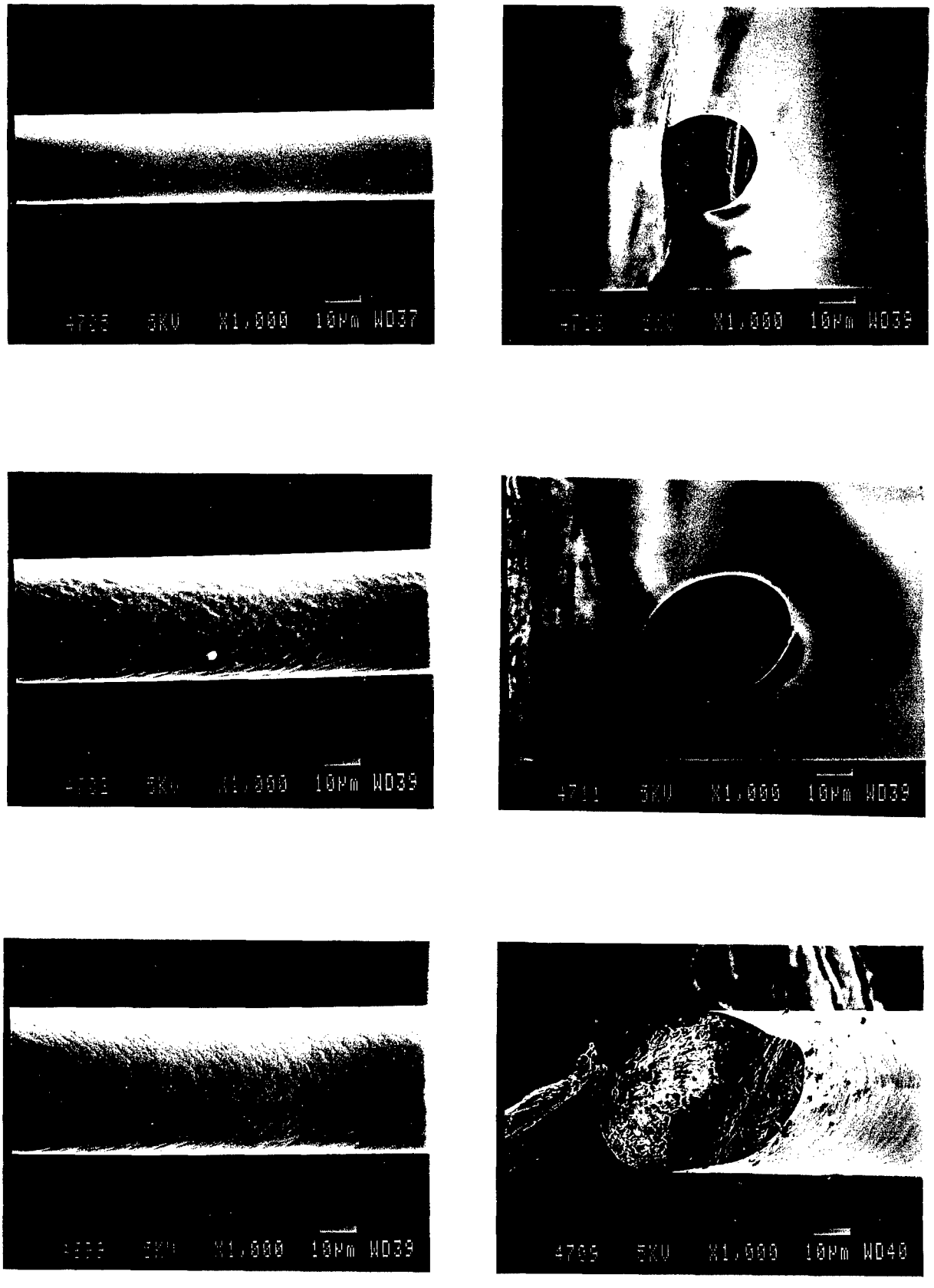

Figure 25. Scanning electron micrograph of mullite-composition fibers crystallized at 1100°C (top) 1200°C, 1300°C, and 1400°C (bottom). Left; longitudinal views, right: sections views. Process time: 15 sec at 1100°C, 30 sec at higher temperatures.

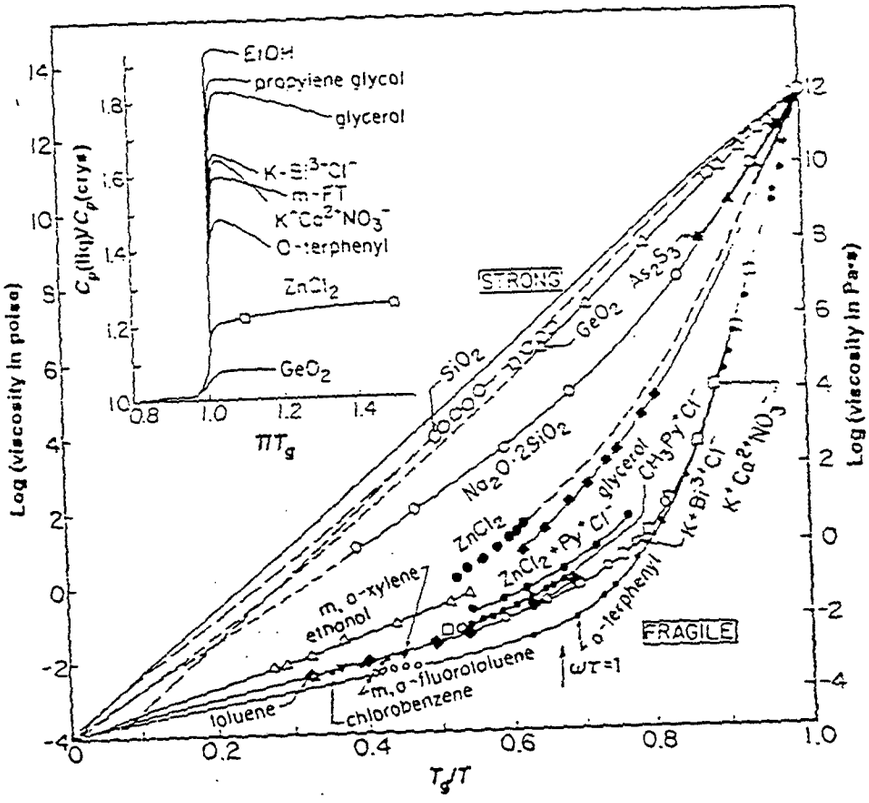

Figure 26. Arrhenius plots for viscosity data scaled by values of Tg for several materials (from reference 21).

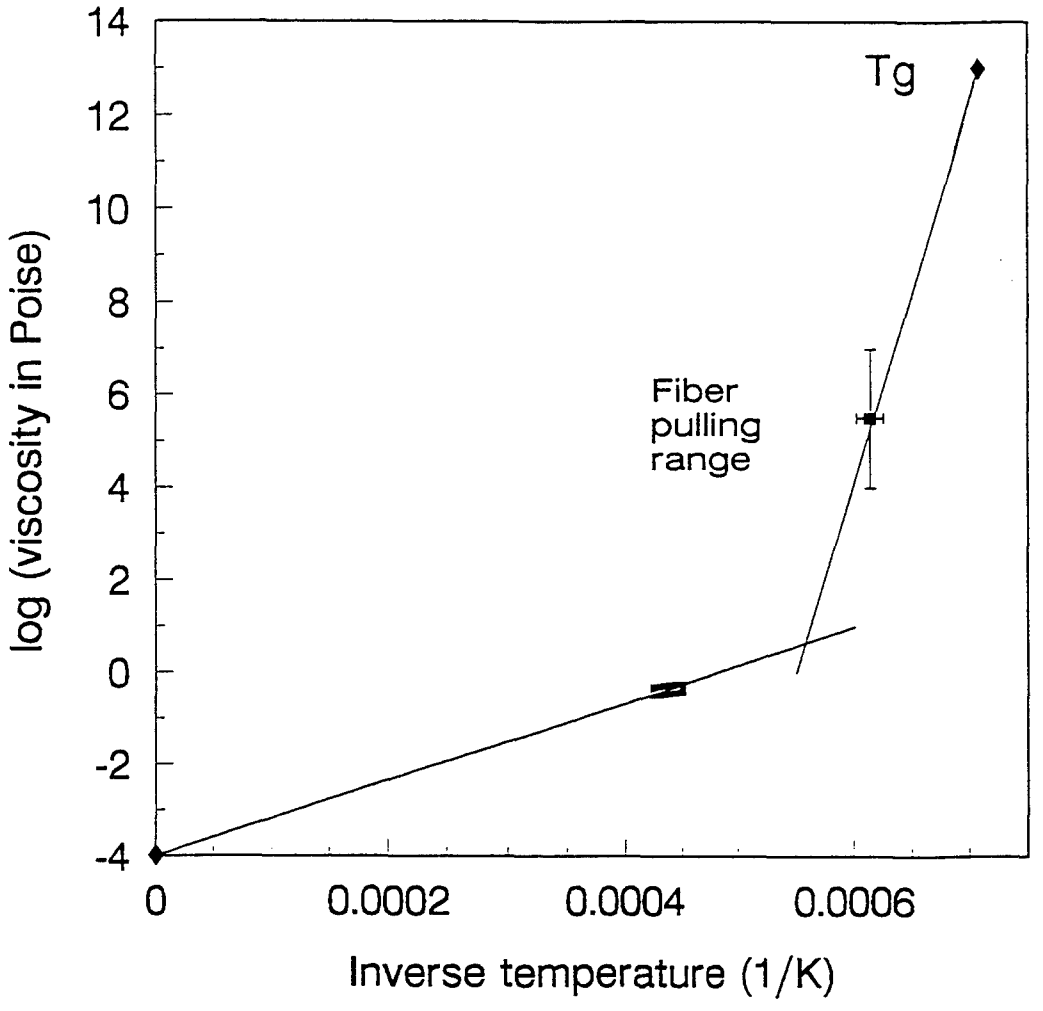

Figure 27. Viscosity of molten YAG *vs* reciprocal temperature from four different sources. The point at $1/T = 0$ is the observation by Angell [18] that liquids exhibit a common intercept at approximately 10^{-4} poise in the plot of log viscosity vs 1/T. The point at 10^{13} poise is at the glass transition temperature of 1150°C by Aasland and McMillan [19]. Data near the melting point are reported by Fratello and Brandle [20]. The viscosity of glass in the working range is plotted at the measured fiber pulling temperature.

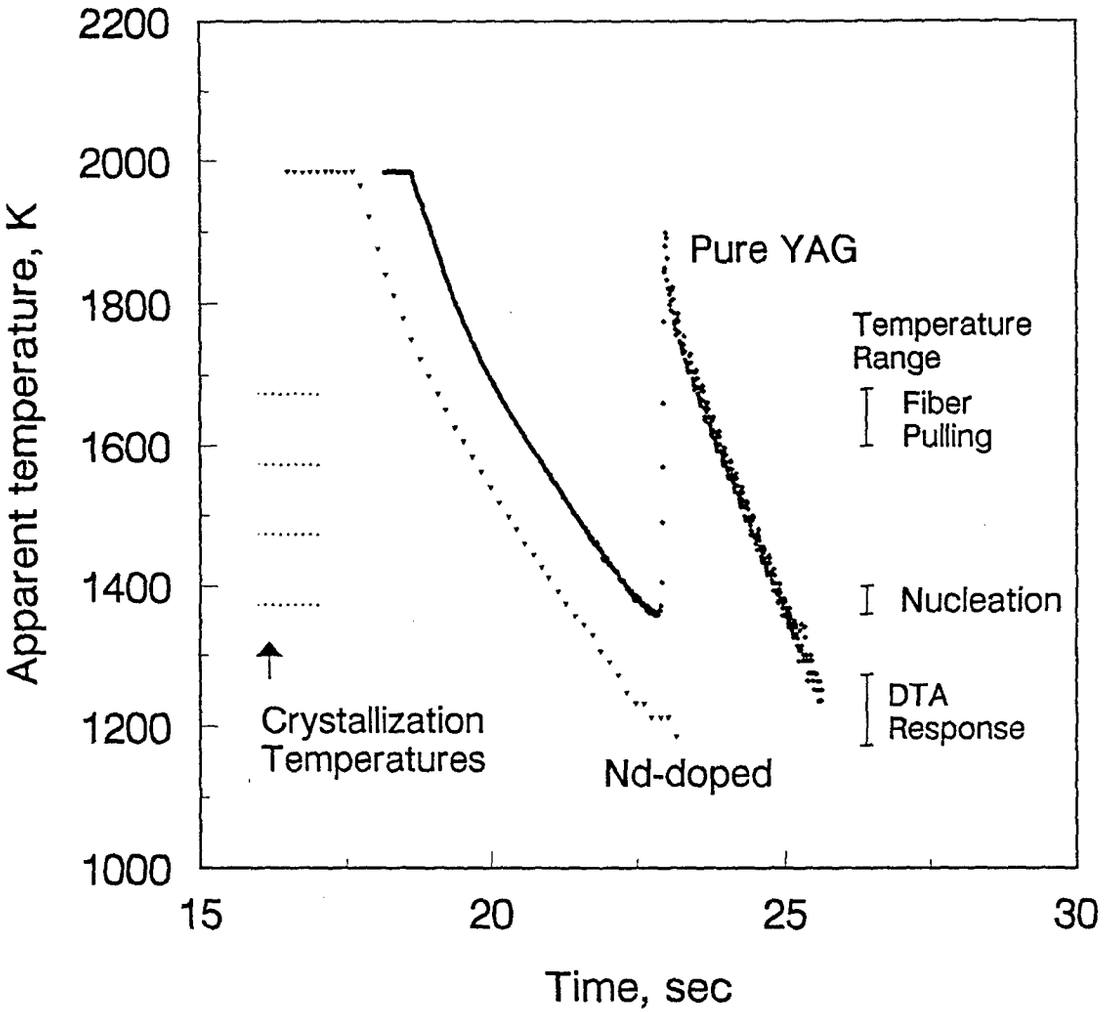

Figure 28. Cooling curves for pure molten YAG and for Nd-doped YAG. Crystal nucleation always occurred in pure molten YAG, typically at a nucleation temperature, T_N in the range 1360-1400K, resulting in a temperature increase of approximately 500K due to the heat released by rapid crystallization of the undercooled liquid. The cooling curve for Nd-doped YAG resulted in glass formation and provides an upper bound on the critical cooling rate for glass formation. The temperature ranges for crystallization in slow heating (DTA) experiments, for nucleation, and for fiber pulling, and the temperatures employed in fast heating crystallization experiments are also shown.

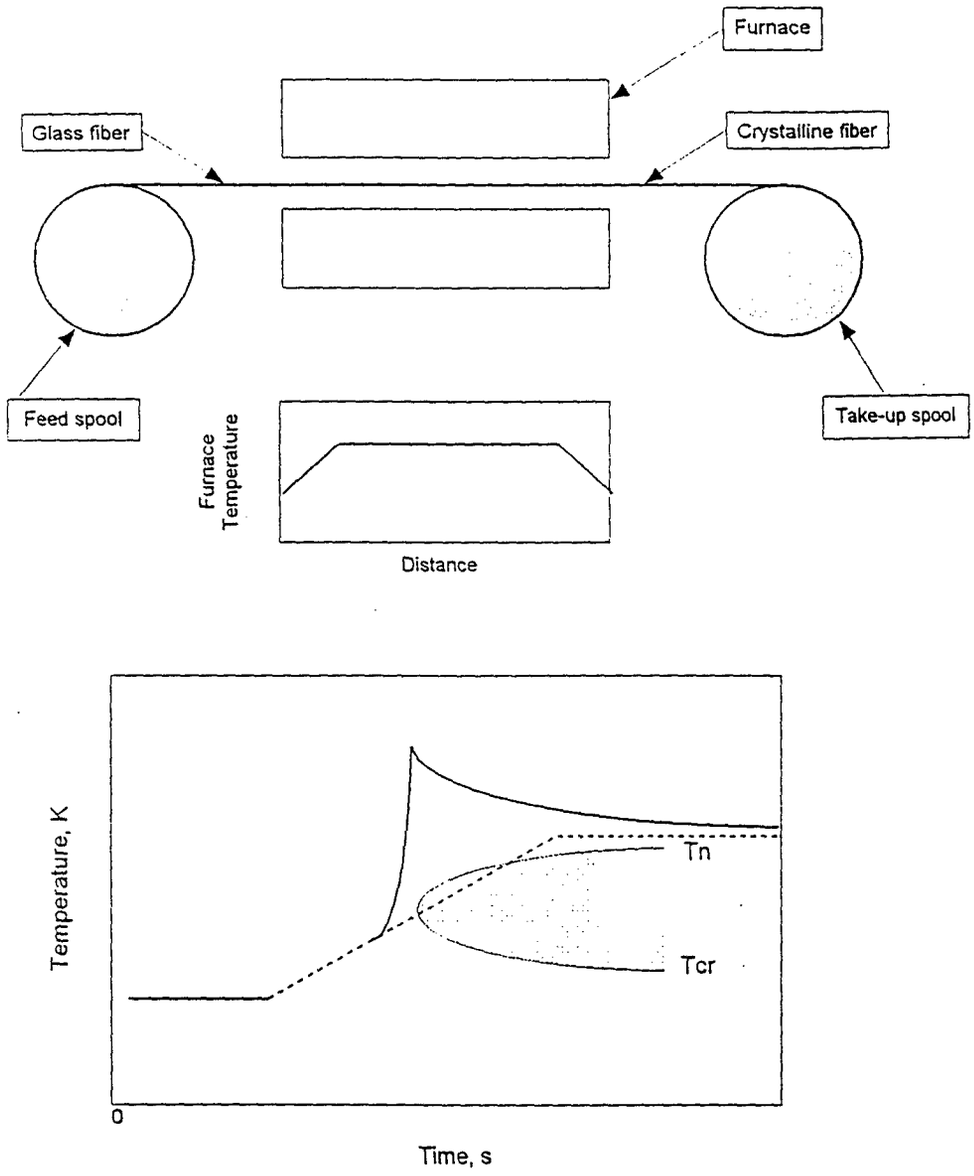

Figure 29. Concept for crystallizing continuous glass fibers. The top part of the figure shows the apparatus, which consists of a small furnace heated to about 1300K, at which temperature the nucleation and growth of crystals from the glass will spontaneously occur. A feed spool feeds glass fiber to the furnace and a take-up spool receives crystalline fiber formed in the furnace. The bottom part illustrates the influence of energy released by the crystallization process on the temperature *vs* time curves for fibers passing through the furnace. (See Section 5.5 for discussion.)